Final Draft
of the original manuscript:

Zeng, R.; Han, E.; Ke, W.; Dietzel, W.; Kainer, K.U.; Atrens, A.:
Influence of microstructure on tensile properties and fatigue crack growth in extruded magnesium alloy AM60
In: International Journal of Fatigue (2009) Elsevier

DOI: 10.1016/j.ijfatigue.2009.07.021

Influence of microstructure on tensile properties and fatigue crack growth in extruded magnesium alloy AM60

R. C. ZENG [a, b*], E. H. HAN [b], W. KE [b], W. Dietzel [c], K. U. Kainer [c], A. Atrens [d]

[a] Chongqing Institute of Technology, Xingsheng Rd. 4, Chongqing, 400050, China

[b] Institute of Metals Research, Chinese Academy of Science, Wencui Rd. 62, Shenyang, 110016,China

[c] GKSS-Forschungszentrum Geesthacht GmbH, Max-Planck-Strasse 1, D-21502 Geesthacht, Germany

[d] The University of Queensland, Division of Materials, Brisbane, QLD 4072 Australia

Abstract

The microstructure, mechanical properties and fatigue crack propagation (FCP) of extruded magnesium alloy AM60 were investigated and compared with rolled AM60. In-situ twinning occurred during fatigue. Denuded zones in the microstructure were attributed to macro-segregation. The observed strain rate sensitivity is attributed to double twinning in the heterogeneous microstructure. Fatigue crack initiation and crack growth is related to slip bands, double twinning and intermetallic compounds for extruded AM60 and to oxide inclusions for rolled AM60. The fracture surfaces of the two materials were distinctly different; small cracks on the fracture surface of rolled AM60 possibly cause crack arrest. Fatigue crack growth of extruded AM60 is dominated by the synergistic influence of the intrinsic microstructure and dislocation-microstructure interactions.

Key words: Magnesium alloy; Intermetallic compounds; Microstructure; Strain-hardening exponent; Fatigue crack nucleation; Fatigue crack growth.

* Corresponding author: Fax: +86-23-68665616
E-mail address: rczeng2001@yahoo.com.cn

1. Introduction

Magnesium alloys have attracted interest as structural materials in the automobile industry due to their low density and adequate strength-to-weight ratio and specific stiffness [1]. Recently, there has been significant effort to improve their mechanical properties. Grain refinement is one approach to increase the yield strength with decreasing grain size according to the Hall–Petch relationship. Grain refined alloys could be produced by hot working by extrusion or rolling. Wrought magnesium alloys have mechanical properties superior to those of castings, particularly ductility and toughness, and consequently are better for stressed components. Therefore, to facilitate the more widespread utilization of magnesium alloys in structural applications, it is necessary to gain better understanding of the relationship between fatigue and microstructure in wrought magnesium alloys.

There has been some prior research on fatigue crack propagation of magnesium alloys [2-6]. Eisenmeier et al [7] claimed that fatigue cracks in cast AZ91 initiate from casting defects that act as stress raisers as did Mayer et al [8] who reported that fatigue cracks initiate at pores in 98.5 % of the samples of high-pressure die-cast AM60. In contrast, Shih et al [9] and Zeng et al [10] found that cracks of extruded AZ61 and AZ80 initiated at inclusions near the specimen surface. Analogous results were also observed on titanium alloys [11]. Previous work of Zeng and co-workers [4, 10, 12] also revealed that fatigue crack growth is significantly influenced by the microstructure. Wrought materials do have sometimes heterogeneous microstructure features, which include lamellar structures, elongated grains, intermetallic compounds and oxide inclusions; these can be at numerous length scales ranging from nanometers to millimeters [13]. These heterogeneities may induce anisotropy in mechanical properties and may influence fatigue. For instance, Xu et al [6] reported that zonal distributed $Mg_3Y_2Zn_3$ in forged Mg-Zn-Y-Zr has an appreciable influence on the fatigue crack propagation rate. Moreover, fatigue crack initiation may be caused by dislocation slip or twining. Nevertheless there is still a lack of knowledge of the influence of twinning on fatigue.

The present study investigated the influence of microstructure on the strain rate sensitivity and fatigue crack initiation and growth of extruded AM60 and rolled AM60. Particular attention was placed on elucidating the microstructure features associated with the fatigue path in order to elucidate the intrinsic fatigue mechanism of magnesium alloys.

2. Experimental

2.1 Materials

The nominal composition of the AM60B is given in Table 1. The rolled reference was produced by rolling 18 mm extruded AM60 plates. They were pre-heated at 500 °C for 1h, hot-rolled at 0.4 mm/pass, to 10 mm with intermediate re-heating at 500 °C for 15min. The rolling direction was parallel to the extrusion direction. The extruded and the rolled materials are designated as AM60-F and AM60-R, respectively.

2.2 Metallography

The specimens for microstructure observations were machined from extruded and rolled plates in three directions: longitudinal (L), long transverse (T) and short transverse (S). The specimens were polished with fine grit emery papers, disc polished using 1 μm diamond powder, washed with acetone and etched in a solution of 10 ml acetic acid, 4.2 g picric acid, 70 ml ethanol and 10 ml distilled water. Microstructure characterization was carried out with an optical microscope. A Philips ESEM×L30 FEG scanning electron microscope (SEM) equipped with energy dispersive spectroscopy (EDS) was employed to characterise fatigue crack surfaces.

2.3. Tensile tests

The plate test specimens, conformed to Standard GB/T16865-1997, with rectangle ends, width 6 mm, thickness 4 mm and gauge length 25 mm. Tensile tests were conducted using a MTS-858 Mini Bionix mechanical test machine at room temperature, using a clip-on extensometer with a gauge length of 25 mm.

2.4. Fatigue tests

The single-notched (notch depth 3.5 mm) specimens of 32 mm by 8 mm cross-section and 150 mm length were machined along the extrusion direction. For fatigue crack growth monitoring, specimens were polished to mirror finish using 1 μm diamond powder for in-situ microstructure observation. Constant load amplitude fatigue crack propagation was studied using an Instron 8500 fatigue machine in ambient air at 16 ºC-20 ºC and 40-70% relative humidity, at a frequency of 1 Hz and a load ratio of zero with a sinusoidal waveform. The crack length, *a,* was measured using a Questa traveling microscope. The stress intensity factor range ΔK was calculated according to [10]. The threshold stress intensity factor range, ΔK_{th} , was obtained by a decreasing load method.

3. Results

3.1. Microstructure

The optical micrographs illustrating the grain structure of extruded and rolled AM60 are presented in Fig.1a and Fig.1b, respectively. The microstructure of extruded AM60 was characterized by twins, banding elongated in the extrusion direction and a grain size ranging from 10 μm to 150 μm with the average grain size of about 56 μm. For rolled AM60, the microstructure consisted of well-defined grains (average grain size ~ 17 μm), a high density of twins and shear bands.

Fig.2a presents a typical SEM micrograph of the macro-segregation of $Mg_{17}Al_{12}$ (indicated with a horizontal arrow) and AlMn particles (indicated with vertical arrows) in extruded AM60. There were denuded zones, devoid of β phase particles at grain boundaries, far from the regions rich in segregated intermetallic compounds in Fig.2b. The smaller particles with square shapes in Fig.3 were identified by EDS to be composed of Al, Mn and a trace of silicon. The atomic ratio of Al: Mn was 1.14:1 indicating these particles were AlMn particles,

originally from the cast alloy.

3.2 Tensile properties

Fig.4 presents typical true stress - true strain curves for extruded AM60 at various strain rates at room temperature. Surprisingly the flow curve was most different at the middle strain rate of 0.147 s^{-1}, whereas the other two curves at the lowest and highest strain rates almost coincided. The ultimate tensile strength (UTS), yield strength (YS) and elongation to failure (EL) of extruded AM60 in the longitudinal direction at various strain rates are presented in Fig.5a, Fig.5b and Fig.5c. The scatter of the data may be attributed to the heterogeneity in microstructure. As the strain rate increased from 5.3×10^{-3} s^{-1} to 1.47×10^{-2} s^{-1}, the UTS and YS increased. However, when the strain rate increased further up to 0.147 s^{-1}, the UTS and YS decreased. It was also unexpected that the ductility also initially increased and later decreased with an increase in strain rate.

In order to evaluate the strain rate sensitivity, the strain hardening exponent, *n*, was determined from the tensile curves. The true flow stress, σ_T, obeys following equation:

$$\sigma_T = k\,\varepsilon_T^{n}, \qquad (1)$$

where

k represents the strength coefficient,

ε_T is the true strain, and

n is the strain-hardening exponent.

The strain-hardening exponent first decreased and then increased as the strain rate increased (Fig.6). Our findings are practically identical with [14-15]. However, Jiang et al [16] reported that the UTS and YS increased and the strain-hardening exponent decreased with increasing strain rate for extruded AM30 and AZ31B. Thus, our experimental results regarding UTS, YS and *n* at a low strain rate range are in agreement with extruded AM30 and AZ31B. The strain hardening behavior is attributed to softening induced by double and contraction

twinning [14, 16]. For the case of the highest strain rate, our results are in good agreement with Takuda et al [15] who observed that the *n* value increased with increasing strain rate for Mg-9Li-1Y at room temperature. In comparison with the literature [17] dealing with the influence of strain rate on the tensile properties of cast AM60, it can be concluded that tensile properties of extruded AM60 are more sensitive to the strain rate. The double twinning in the heterogeneous microstructure may be responsible for this strain rate sensitivity.

3.3. Fatigue crack propagation

The relationship between the fatigue crack propagation rate (FCP), d*a*/d*N*, and the cyclic stress intensity factor range, ΔK, for extruded AM60 and rolled AM60 is presented in Fig.7. Owing to its fine- grained microstructure, the FCP rate of rolled AM60 was considerably faster than that of extruded AM60. It is known that fine-grained material exhibits a higher FCP [18] and a coarser microstructure or/and a more heterogeneous microstructure leads to a lower crack propagation rate [19]. Since the plastic deformation zone in fine-grained material is normally larger than the grain size, a reverse slip of the dislocations during unloading is often impossible and damage accumulation is large during cycling [20]. In particular, for extruded AM60, a knee with two different slopes occurred at ΔK ranges from 5.8 MPa·m$^{1/2}$ to 7.5 MPa·m$^{1/2}$. Similar transitions of slope in d*a*/d*N* vs. ΔK curves occur in other magnesium alloys [21]. The change in slope, however, was reverse compared with what Tokaji et al [22] described, and corresponds to a transition from structure-sensitive to structure-insensitive behavior. The plane-strain mode of FCP can occur at a stress-intensity factor less than half that required for total rupture.

Fig.7 also displays different curves with rather wide scatter of data for similar specimens for extruded AM60. Furthermore, the characteristic plateau range and subsequent acceleration in the curves indicate a decrease in FCP rate of rolled AM60 at a ΔK range of 9 MPa·m$^{1/2}$. This implies crack arrest in the high stress intensity factor range. This unusual phenomena may be related to the microstructural inhomogeneity. The values

(in Table 2) of the threshold stress intensity factor range, $\Delta K_{th,}$ of extruded AM60 reveal that the threshold decreased with an increase in stress ratio; this is similar to our previous work [4].

3.4. Fractography

The overall fatigue crack surfaces of extruded AM60 and rolled AM60 are presented in Fig.8 and Fig.9. Rolled AM60 had a smooth fatigue crack surface, whereas extruded AM60 had a relatively rough fatigue crack surface attributed to the inhomogeneous microstructure. Fig.8a shows a very rough fatigue crack surface with tire tracks that are formed by being cyclically opened, shifted, and pressed together after the fatigue crack front has passed at a lowΔK. Cyclic straining of the fatigue crack surfaces after the fatigue crack has passed causes slip band cracks. Fig.8b is characterized by an extremely rough surface with clear indications of elongated shear dimples and AlMn particles on the bottom of the dimples at a highΔK. It represents the fatigue crack propagation mechanism of micro-void formation and coalescence at the fatigue crack tip. Micro-voids grow from the weak boundaries between AlMn particles and the matrix. Often, their growth and coalescence precludes macroscopic deformation and the absorption of large amounts of energy. Under increasing stress conditions the free surfaces grow into rounded voids, and under sufficient stress they coalesce to form a local increment of fracture. Fig.9a is characterized by a very flat surface with many small embedded cracks which may be related to the high-density of twins developed by rolling at a lowΔK. Tokaji et al [22] proposed that the small cracks initiated within intense slip bands of grains or at grain boundaries due to the fact that the slip bands were blocked by the grain boundaries and thus caused a stress concentration. Tearing voids also existed at a high ΔK in Fig.9b. There is an apparent distinction between two kinds of fatigue cracking: for extruded AM60 with a rougher fatigue crack surface the fatigue crack growth mode underwent a characteristic transition, corresponding to the knee in the da/dN vs. ΔK curves in Fig.7, from plane strain to plane stress (shear) type of fatigue crack propagation mode; whereas, for rolled AM60 with a flat fatigue crack there were no striations.

4. Discussion

Based on these experimental observations, the tensile properties and FCP behavior of the wrought magnesium alloys was associated with the synergistic influence of microstructure and dislocation-microstructure interactions.

4.1 Influence of strain rate on tensile properties

Magnesium exhibits a strong propensity for mechanical twinning because twinning has a lower critical resolved shear stress (CRSS) than <c+a> pyramidal slip at room temperature [16]. Twinning tends to occur in coarse grains instead of fine grains. Twin boundaries, like grain boundaries, act as barriers to dislocation motion, and consequently result in an increase in the work hardening rate. On the other hand, twining accommodates strain along the c-axis, and thus gives rise to a decrease in the work hardening rate [16]. Furthermore, twins decrease with increasing strain [23]. Since the c-axis of the grains are predominantly perpendicular to the tensile direction, twinning needs sufficient time to reorient basal planes to more favorable orientations which in turn leads to softening. Therefore, in the case of a high strain rate, it is difficult for twining to take place. In consequence, grain boundaries and dislocation induced hardening outweigh twinning induced softening, leading to a high strain-hardening exponent.

It was unexpectedly to find that the ductility of extruded AM60 was highest at the middle strain rate. In contrast, extruded AM30 and AZ31B exhibit a decreasing ductility with increasing strain rate [13, 16]. This may be attributed to the inhomogeneous microstructure in which coarse grains and fine recrystallised grains co-exist in extruded AM60. The interaction of softening induced by twinning in coarse grains and hardening induced grain boundaries in fine grains results in a higher ductility and a lower n value at the strain rate of 0.0147 s^{-1}

4.2 Influence of slip bands and twins on FCP

Since the dominant deformation mechanisms in magnesium are basal slip, secondary (prismatic and pyramidal) slip, and $\{10\bar{1}2\}$ tension twinning and $\{10\bar{1}1\}$ compression twinning [24], it is likely that fatigue crack nucleation and growth is controlled by the two factors: dislocation slip and twinning.

In our earlier study [25], slip bands, near the manganese-rich particles and across the crack, as sites for micro-crack initiation; these appeared initially in individual grains with the same crystallographic system, probably basal planes on a pre-polished surface of extruded AM60. It has been also demonstrated that slip bands appear in preferably oriented grains at room temperature in other magnesium alloy such as cast AZ91 [3] and wrought magnesium alloys MA2-1-T2 and MA12-T6 [2].

Anderson et al [24] reported that basal slip occurs first at a stress ~ 0.5 MPa, followed by tension twinning and secondary slip, since basal slip cannot provide five independent slip systems. Twinning is thus the other particularly important cause of crack nucleation in coarse-grained magnesium alloys in a wide temperature range. When the crack and the zone of plastic deformation surrounding the crack tip are confined to within a few grain diameters, crack growth occurs predominantly by single shear, in the direction of the primary slip system [26]. The prevailing crack propagation involves simultaneous or alternating flow along two slip systems. In the present work secondary twining or double twinning also emerged much later than slip bands, and crossed over the crack or appeared far from the crack on the pre-polished and etched surface of extruded AM60 instead of rolled AM60. Fig.10 demonstrates that, near AlMn particles and the fatigue crack, there occurred two types of secondary twinning: A-$(10\bar{1}2)$-$(0\bar{1}\bar{1}2)$ double twinning and B-$\{10\bar{1}1\}$-$\{10\bar{1}2\}$ double twinning [27]. The matrix twins on either a $\{10\bar{1}1\}$ or $\{10\bar{1}2\}$ plane produce a rotation of 38º about the same $<\bar{1}2\bar{1}0>$ axis. The misorientation relationship between $(10\bar{1}2)$ and $(0\bar{1}\bar{1}2)$ planes is responsible for the local maxima in the 50-60º range with a clustering of rotation axes near $<0\bar{1}\bar{1}2>$ [16, 27]. $\{10\bar{1}2\}$ twinning occurred on two different $\{10\bar{1}2\}$ planes in a considerable fraction of grains. A type secondary twinning is the predominant

deformation mode in tension-zero-tension fatigue crack propagation.

It is not the case for rolled AM60. There was no twinning but branching and small cracks on pre-polished and etched specimen of rolled AM60 [25]. There may be three reasons:

(i) the propensity for twinning decreases with decreasing grain size. Twinning occurs preferentially in coarse grains due to their lower CRSS. It is suggested that there exists a critical grain size below which deformation twinning at room temperature is suppressed [28]. For instance, this critical size in ZK60 processed by warm equal channel angular extrusion (ECAE) is approximately 3-4 μm [28]. The grain size of rolled AM60 was smaller than that of extruded AM60. As a result, secondary twinning does not easily occur in rolled AM60.

(ii) Crack closure, which developes compressive stresses, is not as strong in rolled AM60 as in extruded AM60. $\{10\bar{1}2\}$ twinning is caused by tension and $\{10\bar{1}1\}$ twinning results from compression. $\{10\bar{1}2\}$ twinning could occur in both c-axis extension and compression [27]. No compressive stress was exerted in the fatigue machine, provided that the tests were conducted under zero-tension loading. What gives rise to $\{10\bar{1}1\}$ twinning? The answer is probablly that crack closure produces the compressive stress.

(iii) Texture may have some impact on twinning. For rolled AM60, unidirectional rolling in the L-direction causes the basal planes (0001) to align parallel to the rolling plane, whereas, for extruded AM60, most of the grains were oriented with the basal planes parallel to the extrusion direction and normal to the surface of the extrusion [20].

4.3 Influence of grain boundaries on FCP

GBs play a dual role in FCP. On one hand, crack branching, in most cases, takes place at GBs. For example, Tokajiet al [22] found that fatigue cracks initiated within grains (transgranular) or at GBs (intergranular) for rolled AZ31. Yue et al [29] demonstrated that, for squeeze cast AZ91, transgranular fatigue cracks frequently

changed direction at GBs. The amplitude of crack deviation was much greater in coarse grain specimens. This indicates that GBs inhibit fatigue crack propagation. On the other hand, GBs behaves like an obstacle. Micro-voids therefore evolved at the triple GBs. Fig.11 depicts the crack tip of extruded AM60 at a high ΔK of 11.0MPa.m $^{1/2}$. Fig.11a shows micro-voids occurring at GBs in the plastic deformation zone oriented at 45° to the direction of applied stress. Because the plastic deformation zone is bigger than the grain size, it was difficult for several grains to accommodate. Fig.11b shows that three micro-voids emanated in the interior of the grain at the fatigue crack tip, indicating that fatigue crack growth was induced by coalescence of micro-voids. This FCP mechanism of micro-voids coalescence has been discussed in our previous study [12].

4.4. Influence of second-phase particles on FCP

The intermetallics $Mg_{17}Al_{12}$ and AlMn, just as GBs, have a crucial influence on the FCP behavior. Crack nucleation at secondary particles can lead either to de-cohesion of the particle-matrix interface or to cracking of the inclusion. Both of these micro-cracks have been observed experimentally. These particles are obviously a potential source of void formation.

4.4.1. Influence of β phase on FCP

Fig.12a exhibits a fatigue crack path across the macro-segregation areas of the β-phase in extruded AM60. Aluminum-rich alloying of these zones may cause lamellar shaped β-phase areas. The crack in extruded AM60 predominately tends to propagate along the lamellar direction of the β-phase (Fig. 12b). Precipitated β-phase in extruded AM60 exhibits a lamellar structure, which is similar to pearlite in carbon steels. Bowles [19] mentioned that the fractured lamella Fe_3C in 0.65%C wheel steel result in voids that link up to form a continuous fracture. The fatigue crack advanced towards the direction perpendicular to iron carbide lamellar. Fig.7 reveals the change in slope of the FCP in extruded AM60, probably and partially concerning the successive occurrence of macro-segregation β-phase on the fatigue crack propagation path.

4.4.2. Influence of AlMn particle on FCP

The other intermetallic compounds such as the manganese-rich particles in magnesium alloys may play a dual role: (1) promoting crack nucleation through the formation of micro-voids and micro-cracks and (2) thwarting the FCP via deflection and branching of the crack path.

Fig.13a indicates a micro-crack nucleated at AlMn particles on the fatigue crack surface of extruded AM60 at ΔK of 4.9MPa.m $^{1/2}$. An analogous result obtained by Uematsu [30] proposed that Al-Mn intermetallics are the crack initiation sites for AZ80. However, Bowles and others [19] pointed out that fatigue cracks of 7XXX series aluminum alloys generally initiated at larger inclusions, which were larger than the usual second-phase particles. Accordingly, the fatigue crack growth, in extruded AM60, advances through void formation induced by AlMn particles ahead of the advancing fatigue crack tip.

AlMn particles cause cyclic deflection and branching of the fatigue crack path depending on the grain size and on the homogeneity of the microstructure (Fig.13b). Because the AlMn particles are too hard to be cracked, the fatigue crack has to deflect or branch, even in cases where the fatigue crack runs across a cluster of these hard particles. Deflection and branching of the fatigue crack path is also apparently in Fig.14. That means that, just like the β phase, the particles may slow the crack growth rate. However, the degree of the deflection caused by AlMn particles is limited due to their small size. Hence, the influence of AlMn phase on FCP rate is limited and may be less than that of the β phase.

4.5 Influence of plastic zone on FCP

For extruded AM60 with average yield strength, σ_y, of 145 MPa and a stress intensity factor of 7.6 MPa.m $^{1/2}$, the maximum process zone size in plane strain can be estimated as [26]:

$$r_p = \frac{1}{6\pi}\left(\frac{K_{\max}}{\sigma_y}\right)^2 = 146\ \mu\text{m} \qquad (2)$$

A maximum process zone of 146 μm corresponds approximately to the biggest grain size 150 μm in

extruded AM60. Consequently, the transition in growth mechanisms is attributed to a switch in growth mechanism from plane strain to plane stress.

4.6. Influence of oxide on FCP

Fig.9a demonstrates numerous secondary cracks, which are parallel to the fatigue crack growth direction and perpendicular to the fatigue crack surface of rolled AM60. The cracks seem to initiate at oxides. Oxides as inclusions are normally found in metallic materials, especially reactive metals like magnesium alloys which are easily oxidized due to their higher chemical activity with oxygen. A complete prevention of oxide inclusions is difficult. Moreover, rolled AM60 was heated directly in air at elevated temperature before rolling, and it was quite likely that the oxide film was rolled into the grain interiors. It has been demonstrated that in many cases oxides were the nucleation sites of fatigue cracks in magnesium alloys. For examples, fatigue cracks nucleated at trapped oxides at near surface of an extruded AZ80 [31] and AZ91E [18]. Furthermore, these micro-cracks can result in fatigue crack arrest, which may be indicated in the FCP rate vs. ΔK curves of rolled AM60 in Fig.7.

4.7 Influence of crack closure on FCP

Surface roughness and oxidation of the fatigue crack are known to produce crack closure [26]. Regardless of the closure mechanism, the effect is to reduce the strain amplitude at the crack tip so as to reduce the crack growth rate compared with a closure-free crack. In the present experiments, Fig. 14 shows large crack deflection and crack branching of extruded AM60. At lower ΔK and an R ratio of zero, the maximum height of the fracture surface asperities reached 88 μm, which is comparable to the average grain size of 56 μm. In Fig.14, the fatigue crack advanced from left to right and at a point "A" stopped propagating on the surface while it continued inside the specimen. It grew around some material heterogeneity, e.g., grain boundaries ① and ②, and it reappeared at B, C…G and continued propagation on the surface but on a shifted plane. Thus, the two fracture surfaces are

locally connected (bridged) and their relative displacement is restrained, which has an obvious shielding on the crack tip. This similar phenomenon was also observed in coarse-grained magnesium [32]. The FCP rate of extruded AM60 is much lower than that of rolled AM60 in the first stage, because of a roughness induced crack closure (RICC) contribution to the decrease in crack growth of extruded AM60. The da/dN-ΔK curves (Fig.7) show transition, plateau and retardation, and subsequent acceleration in crack growth with increasing cyclic stress intensity factor range. The explanation lies in following aspects: (1) crack deflection and crack branching at grain boundaries and/or precipitates such as AlMn particles. The crack deflection from its normal growth plane reduces the effective stress intensity factor at the crack tip, which decreases FCP rate. (2) The plastic deformation zone is smaller than the coarser grain size and/or the β-colony range (Fig.12). The resistances exerted by the β-colonies and no favorably oriented neighboring grains retard crack propagation. (3) For the oscillatory crack growth phenomena of rolled AM60, small fatigue crack initiation (Fig.9a) consumes a part of the driving force. (4) Reduced fatigue crack growth may be partly attributed to crack closure.

4.8 Crack propagation model

A fatigue crack propagation model is presented to explain the mechanism of FCP in Fig.15, based on the above observation of the microstructure.

(1) Firstly, dislocations pile up at GBs, slip bands occurring along the orientation of 45º to the strain plane with increasing micro-plastic deformation.

(2) And then a fatigue crack may nucleate at a slip band;

(3) The fatigue crack propagates along GBs, if it runs across small grains. Otherwise, the fatigue crack advances in a transgranular mode across the coarse grains;

(4) At the higher ΔK levels, macro-cracks may nucleate at intermetallic particles/ GBs;

(5) On GBs or precipitates, such as AlMn particles, the fatigue crack is deflected and branched.

(6) Primary twinning and secondary twinning developed in the coarser grains.

(7) When reaching a β-lamella colony, the fatigue crack grows with a tendency to be parallel to the β-lamella; otherwise, the fatigue has to propagate across the lamellae.

(8) In most cases, the fatigue crack moves forward along the opened twins in the interior of the coarse grains.

(9) At the very high ΔK, micro-voids evolve ahead of the crack tip, and coalescence of these voids advances a fatigue crack. Shear dimples can be easily observed on the fatigue surface.

(10) Finally, the fatigue crack propagates at a mixed transgranular and intergranular mode.

5. Conclusions

An investigation into the microstructure, mechanical properties and FCP behavior of extruded AM60 has been performed in comparison with rolled AM60. The followings are the salient observations:

(1) Extrusion of AM60 leads to a inhomogeneous grain structure consisting of large elongated and small-recrystallised grain fractions. Macro-segregation of second-phase particles/constituent particles results in denuded zones that are depleted of particles at GBs.

(2) The mechanical properties of extruded AM60 illustrates that extruded material is relatively sensitive to the applied strain rate, compared with cast AM60. The strain hardening exponent, n, of extruded AM60 declined with increasing strain rate from 5.3×10^{-3} s^{-1} to 0.0147 s^{-1}, whereas, the n value increased in the strain rate range of 0.0147 s^{-1} and 0.147 s^{-1}. Double twinning in the heterogeneous microstructure are predominantly responsible for these findings.

(3) Fatigue crack initiation and advance was related to the synergistic influence of slip bands, double

twinning, intermetallic compounds and grain boundaries for extruded AM60 and to oxides for rolled AM60. There were two types of double twinning near AlMn particles and fatigue cracks during fatigue propagation of extruded AM60 due to the localized coarser grains in the microstructure. In addition, intermetallic particles bring about crack deviation and branching; hence exert an influence on the fatigue crack propagation rate dependant on particle size. There was a distinct difference of the fatigue crack surfaces: extruded AM60 had a rough fatigue crack surface caused by cleavage and shear voids, whereas rolled AM60 developed a flat fatigue crack surface. Small cracks resulted from oxide on the fatigue crack surface of rolled AM60 may responsible for oscillatory crack growth and crack arrest.

(4) A model established to interpret the fatigue crack nucleation and growth imposes limitations upon the examinations into the untypical extruded materials. Nevertheless, this study reveals a comprehensive and systematic understanding into the FCP mechanism of magnesium alloys.

Acknowledgements

The National Hi-Tech Research and Development Program supported this work under grant No.2001AA331050. Thanks go to Guangling Magnesium Industry Science and Technology Co. Ltd. for providing the tested materials and to Prof. Gao Guozhong in Institute of Metals Research, Chinese Academy of Science for the help on the rolling process.

References

[1] Zeng RC, Dietzel W, Zettler R, Chen J, Kainer KU. Microstructure evolution and tensile properties of friction-stir-welded AM50 magnesium alloy. Trans. Nonferrous Met. Soc. China 2008; 18: s76-s80.

[2] Ogarevic VV, Stephens RI. Annu. Fatigue of magnesium alloys. Rev. Mater. Sci. 1990; 20: 141.

[3] Potzies C, Kainer KU. Fatigue of magnesium alloys. Adv. Eng. Mater. 2004; 6(5): 281-289.

[4] Zeng RC, Han EH, Ke W. Fatigue and Corrosion Fatigue of Magnesium Alloys. Mater. Sci. Forum 2005; 488-489: 21-724.

[5] Lee SG, Patel G.R, Gokhale AM. Inverse surface macro-segregation in high-pressure die-cast AM60 magnesium alloy and its effects on fatigue behavior. Scripta Mater. 2005; 52: 1063-1068.

[6] Xu DK, Liu L, Xu YB, Han EH. The fatigues crack propagation behavior of the forged Mg-Zn-Y-Zr alloy. J. Alloy & Compd. 2007; 431(1-2): 107-111

[7] Eisenmeier G, Holzwarth B, Hoeppel HW, Mughrabi H. cyclic deformation and fatigue behavior of the magnesium alloy AZ91. Mater. Sci. Eng. A 2001; 319-321: 578-582.

[8] Mayer H, Papakyriacou M, Zettl B, Stanzl-Tschegg SE. High cycle fatigue mechanisms in a cast AM60B magnesium alloy. Inter. J. Fatigue 2003; 25: 245-256.

[9] Shih TS, Liu WS, Chen YJ. Fatigue of as-extruded AZ61A magnesium alloy. Mater. Sci. Eng. A 2002; 325: 152-162.

[10] Zeng RC, Ke W, Han EH. Influence of load frequency and ageing heat treatment on fatigue crack propagation rate of as-extruded AZ61 alloy. Inter. J. Fatigue 2009; 31(3): 463–467.

[11] Atrens A, Hoffelner W, Duerig TW, Allison JE. Subsurface crack initiation in high cycle fatigue in Ti6Al4V and in a typical martensitic stainless steel. Scripta Metallurgica 1983; 17: 601-606.

[12] Zeng RC, Xu YB, Han EH, Ke W. Fatigue crack propagation behavior of as-extruded magnesium alloy AZ80. Mater. Sci. & Eng. A, 2009, doi:10.1016/j.msea.2009.01.013.

[13] Nan ZY, Ishihara S, Goshima T. Corrosion fatigue behavior of extruded magnesium alloy AZ31 in sodium chloride solution. Inter. J. Fatigue 2008; 30: 1181-1181.

[14] Lin XZ, Chen DL. Strain hardening and strain-rate sensitivity of an extruded magnesium alloy. JMEPEG 2008; 17: 894-901.

[15] Takuda H, Kikuchi S, Yoshida N, Okahara H. Tensile properties and press formability of a Mg-9 Li-1 Y alloy sheet. Mater. Trans. 2003; 44(11): 2266-2270.

[16] Jiang L, Jonas JJ, Luo AA, Sachdev AK, Godet S. Twinning-induced softening in polycrystalline AM30 Mg alloy at moderate temperatures. Scripta Mater. 2006; 54(5): 771-775.

[17] Abbott T, Easton M, Song W. Mechanical behavior of cast magnesium alloys. Mater. Sci. Forum 2003; 419-422: 93-102.

[18] Horstemeyer MF, Yang N, Gall K, McDowell D L, Fan J, Gullett PM. High cycle fatigue of a die cast AZ91E-T4 magnesium alloy. Acta Mater. 2004; 52: 1327-1336.

[19] Bowles CQ. Fracture and structure, Fatigue and Fracture, Vol.19, ASM handbook, Lampman SR, editor. Materials Park (OH): ASM International, 1996, pp.5-8.

[20] Mukai T, Watanabe H, Ishikawa K, Higashi K. Guide for enhancement of room temperature ductility in Mg alloys at high strain rates. Mater. Sci. Forum 2003; 419-422: 171-176.

[21] Sajuri Z B, Miyashita Y, Hosokai Y, Mutoh Y. Inter. Effect of Mn content and texture on fatigue properties of as-cast and extruded AZ61 magnesium alloys. J. Mechanical Sci. 2006; 48: 198-209.

[22] Tokaji K, Kamakura M, Ishiizumi Y, Hasegawa N. Fatigue behavior and fracture mechanism of a rolled AZ31 magnesium alloy. Inter. J. Fatigue 2004; 26: 1217-1224.

[23] Barnett MR, Nave MD, Bettles CJ. Deformation microstructures and textures of some cold rolled Mg alloys. Mater. Sci. & Eng. A 2004; 386: 205-211.

[24] Andersson P, Caceres CH, Koikke J. Hall-Petch parameters for tension and compression in cast Mg. Mater. Sci. Forum 2003; 419-422: 123-128.

[25] Zeng RC, Han EH, Liu L, Xu YB, Ke W. Effect of rolled microstructure on fatigue properties of magnesium alloy AM60. Chinese J. Mater. Research 2003; 17(3): 241-245.

[26] Suresh S. Fatigue of materials. Cambridge: Cambridge University Press, 1998, pp. 609-610.

[27] Nave MD, Barnett MR. Microstructure and texture of pure magnesium deformed in plane-strain compression. Scripta Mater. 2004; 51: 881-885.

[28] Lapovok R, Thomson PF, Cottam R. The effect of grain refinement by warm equal channel angular extrusion on room temperature twinning in magnesium alloy ZK60. J. Mater. Sci. 2005; 40: 699-1708.

[29] Yue TM, Ha H, Musson NJ. cyclic deformation and fatigue behavior of the magnesium alloy AZ91. J. Mater. Sci. 1995; 30: 2277-2283.

[30] Uematsu Y, Tokaji K, Kamakura M, Uchida K, Shibata H, Bekku N. Effect of extrusion conditions on grain refinement and fatigue behavior in magnesium alloys. Mater. Sci. & Eng. A 2006; 434: 131–140.

[31] Zeng RC, Han EH, Ke W, Liu L, Xu YB. Mechanism of corrosion fatigue for as-extruded magnesium alloy AZ80. Chinese J. Mater. Research 2004; 18(6): 561-567.

[32] Nicoletto G, Konecna R, Pirondi A. Fatigue crack paths in coarse-grained magnesium. Fatigue Fract. Eng. Mater. Struct. 2005; 28: 237-244.

Figure captions

Fig.1 Microstructures of (a) extruded AM60 and (b) rolled AM60.

Figs.2 SEM micrograph of (a) macro-segregation of $Mg_{17}Al_{12}$ (indicated by horizontal arrow) and Al-Mn particles (indicated by vertical arrows) in extruded AM60; (b) the denuded zones without $Mg_{17}Al_{12}$ precipitates.

Fig.3 Chemical composition of the AlMn phase in AM60 identified with EDS.

Fig.4 True stress-strain curves at various strain rates for extruded AM60

Fig.5 Mechanical properties: (a) Ultimate tensile strength (UTS), (b) yield strength (YS) and (c) elongation of extruded AM60 as a function of the strain rate.

Fig.6 Influence of strain rate on the strain-hardening exponent, *n*, for extruded AM60.

Fig. 7 FCP rate versus □*K* curves for extruded AM60 and rolled AM60.

Fig.8 Fractographic observation showing fracture surfaces for extruded AM60: (a) tire tracks at a low Δ*K* level; (b) AlMn particles on the bottom of shear dimples at a high Δ*K* level.

Fig.9 SEM micrographs showing flat fracture surfaces for rolled AM60: (a) oxide and numerous secondary macro-cracks at a low Δ*K* level. (b) No apparent dimples at a high Δ*K* level.

Fig.10 Optical micrographs of two types of double twinning: A type- (1012)-(0112) twinning and B type- {1011}-{1012 } twinning near AlMn particles and crack. Deflection and branches are also found on the surface.

Fig.11 (a) SEM morphology of extruded AM60 at crack tip at high-rate region (ΔK = 11.0MPa.m 1/2). Micro-voids (indicated with horizontal arrows) occurred at triple grain boundaries in plastic deformation zone at an angle of 45˚ with crack. (b) Magnification of area A, crack tip is formed by coalescence of micro-voids (indicated with vertical arrows).

Fig. 12 (a) Scanning electron micrographs of macro- segregation of $Mg_{17}Al_{12}$ phase polished surface of extruded AM60 after FCP, (b) high magnification of area A in (a) showing a macroscopic cracking in lamellar *β* phases.

Fig.13 Fractographs revealing (a) a micro-crack emanating at an AlMn particle (indicated with a vertical arrow), which itself do not crack, on the fracture surface of the extruded AM60 sample at Δ*K* of 4.9 MPa.m $^{1/2}$, (b) fatigue crack deflection and branch caused by AlMn particles in the extruded AM60 alloy.

Fig.14 Crack growth profile, of extruded AM60, showing grain boundaries such as ① and ②, and

branching such as A, B and C along the crack.

Fig.15 Schematic model for fatigue crack propagation in extruded AM60.

Table captions

Table 1 Nominal composition of magnesium alloy AM60, wt %

Table 2 Values of threshold stress intensity factor range, ΔK_{th}, of the extruded materials.

Table 1

Al	Mn	Si	Fe	Cu	Ni	Mg
5.60-6.40	0.26-0.50	≤0.05	≤0.004	≤0.008	≤0.001	Balance

Table 2

Load ratio R	0	0.2
ΔK_{th}	<2.24	<1.55

Figure(s)1a

Click here to download high resolution image

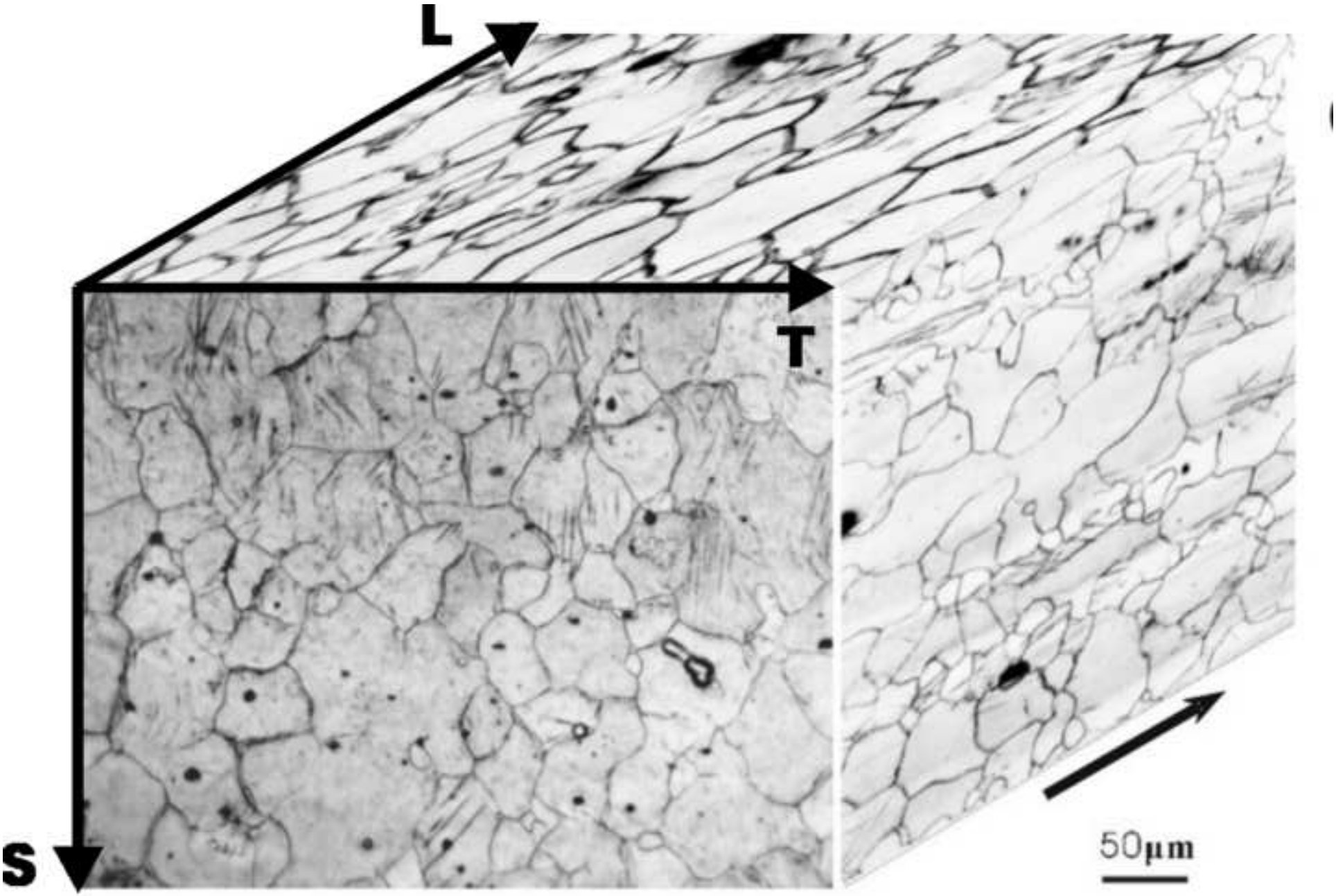

Figure(s)1b

Click here to download high resolution image

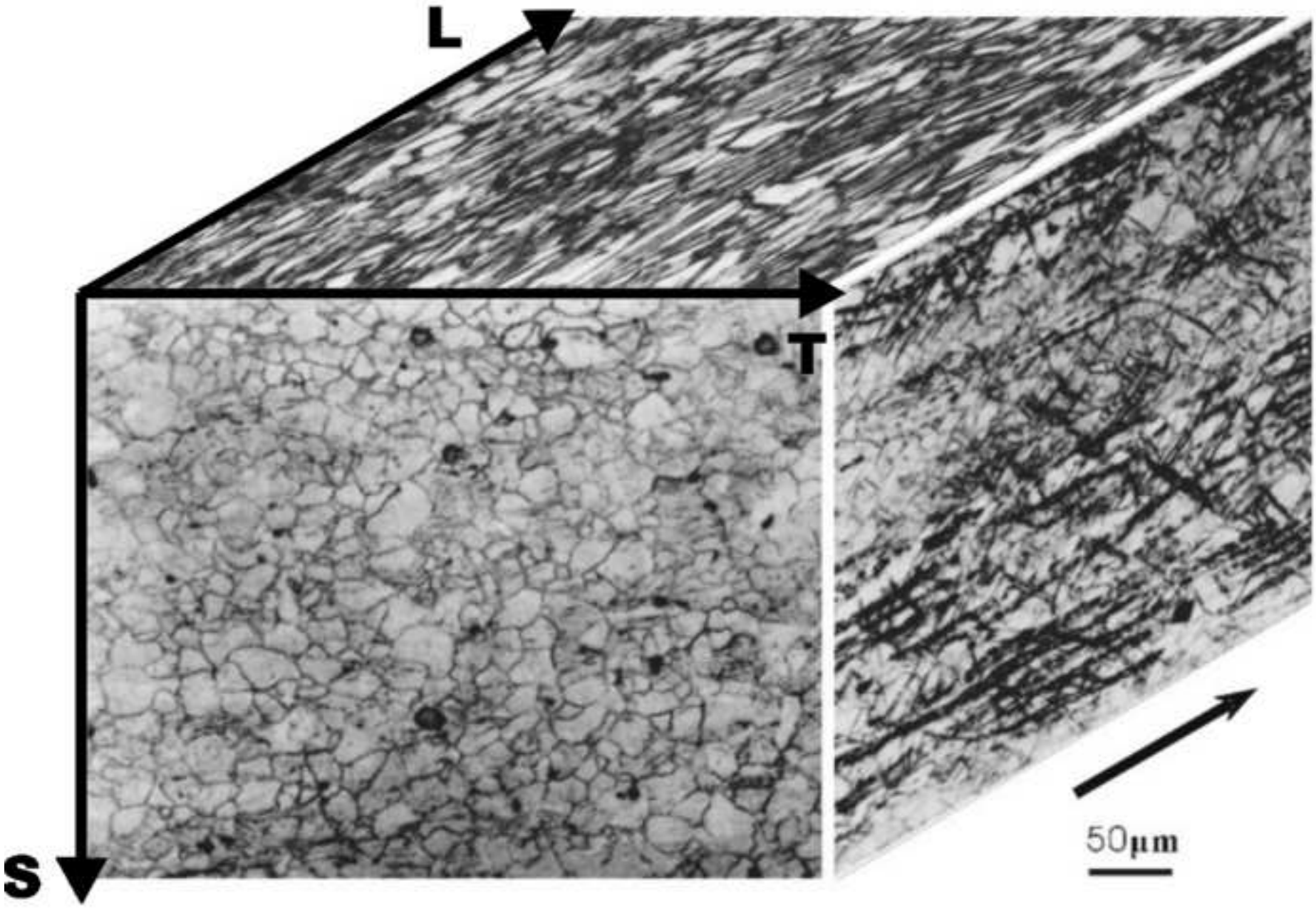

Figure(s)2a

Click here to download high resolution image

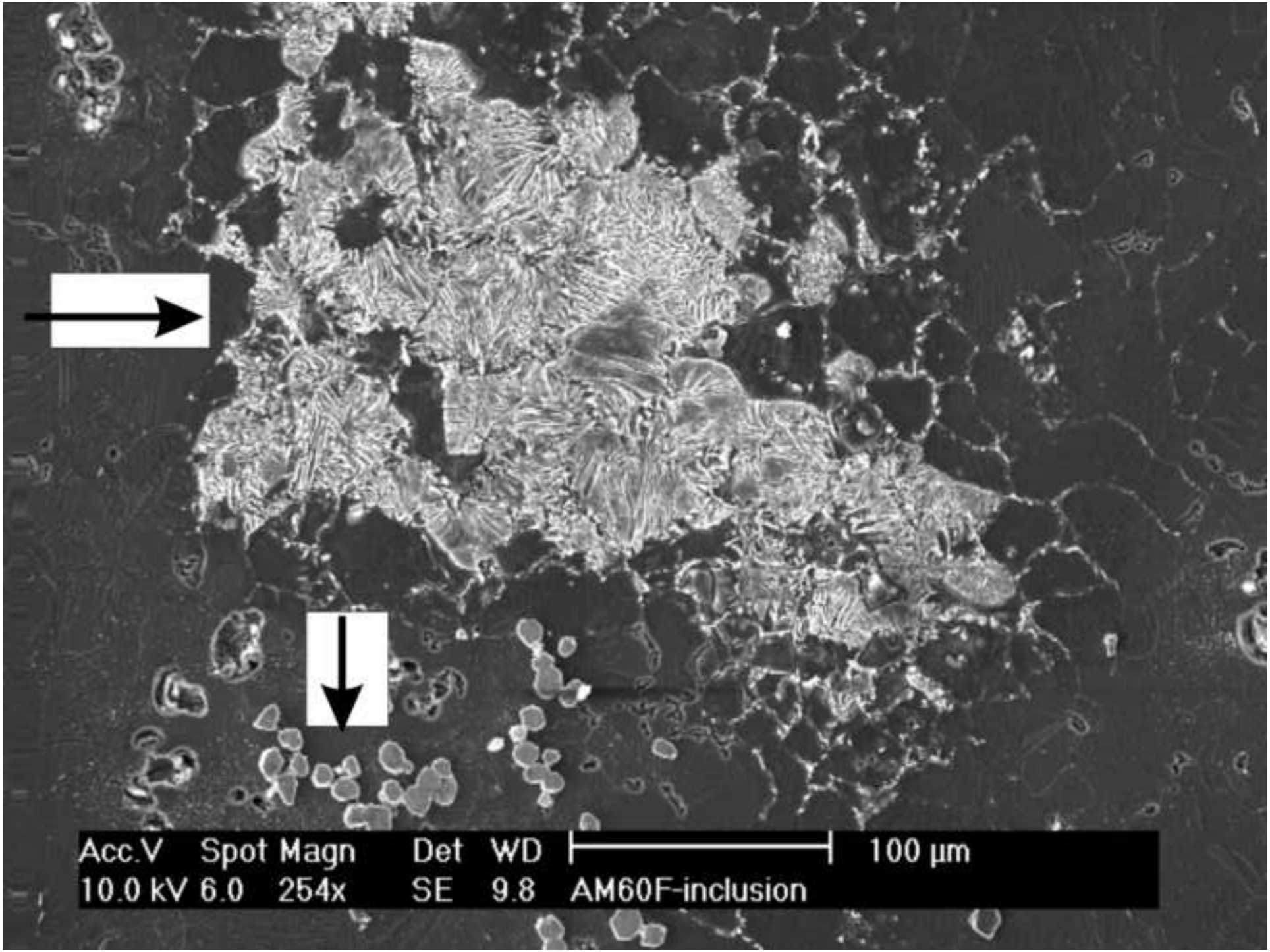

Figure(s)2b

Click here to download high resolution image

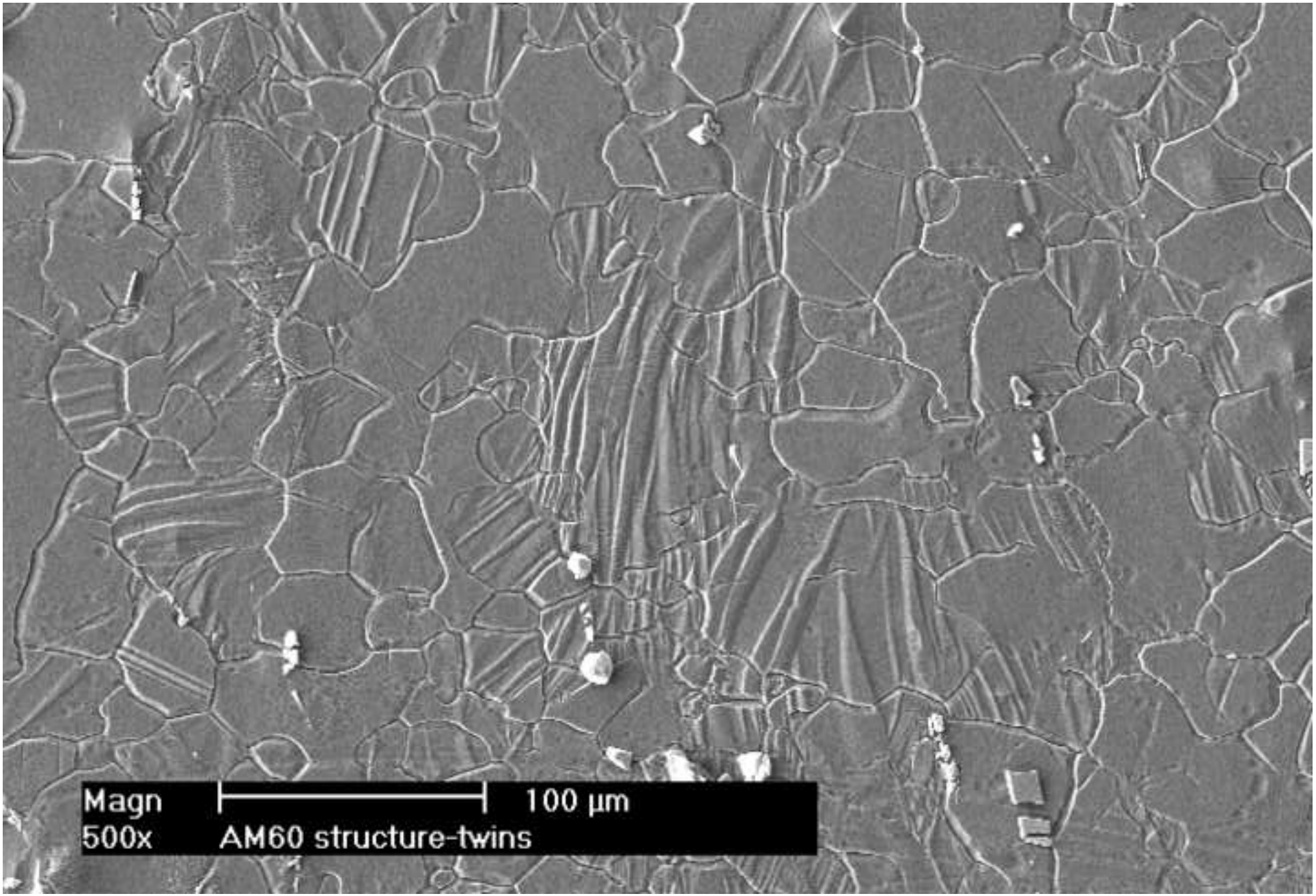

Figure(s)3

Click here to download high resolution image

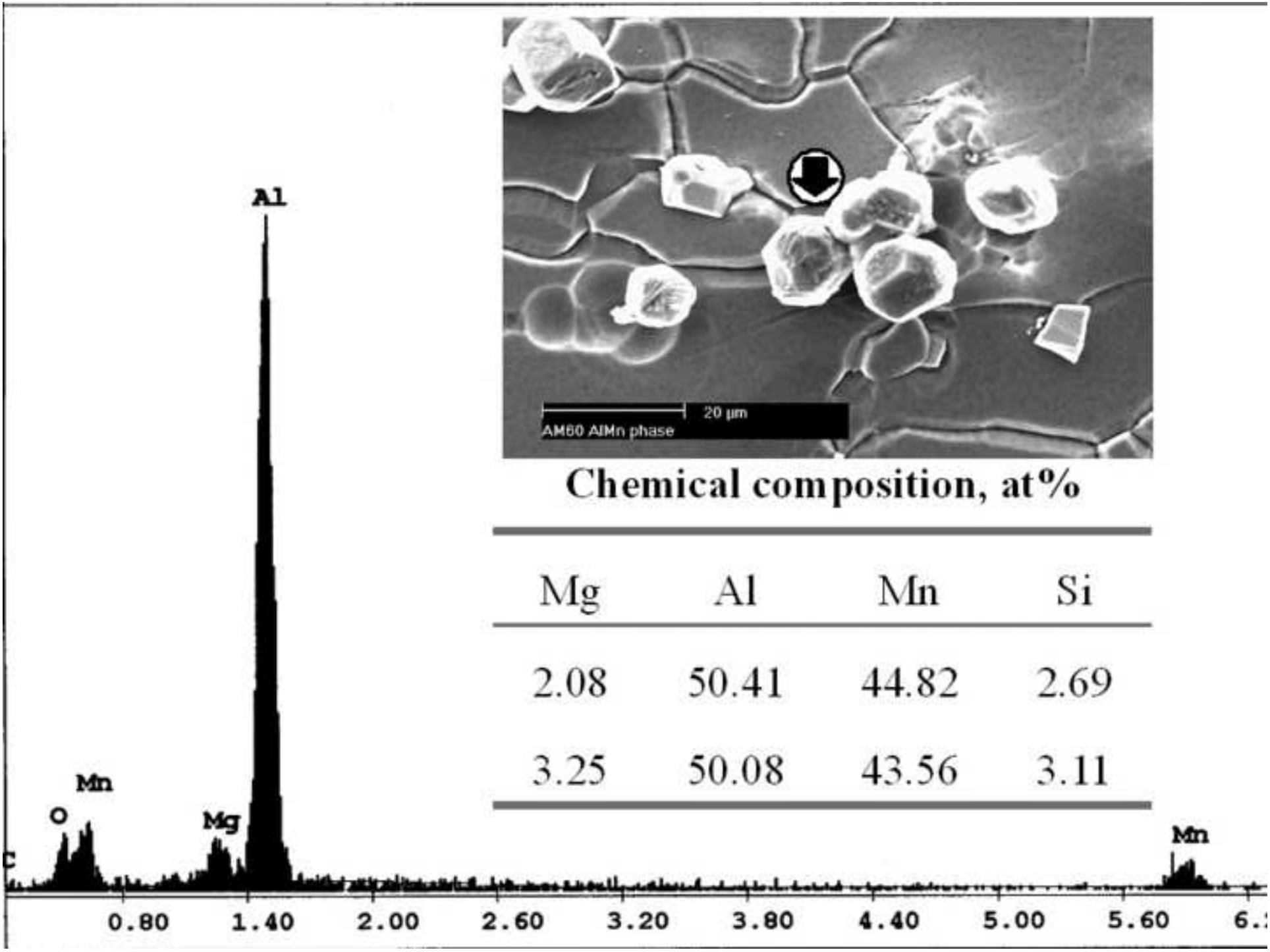

Chemical composition, at%

Mg	Al	Mn	Si
2.08	50.41	44.82	2.69
3.25	50.08	43.56	3.11

Figure(s)4

Click here to download high resolution image

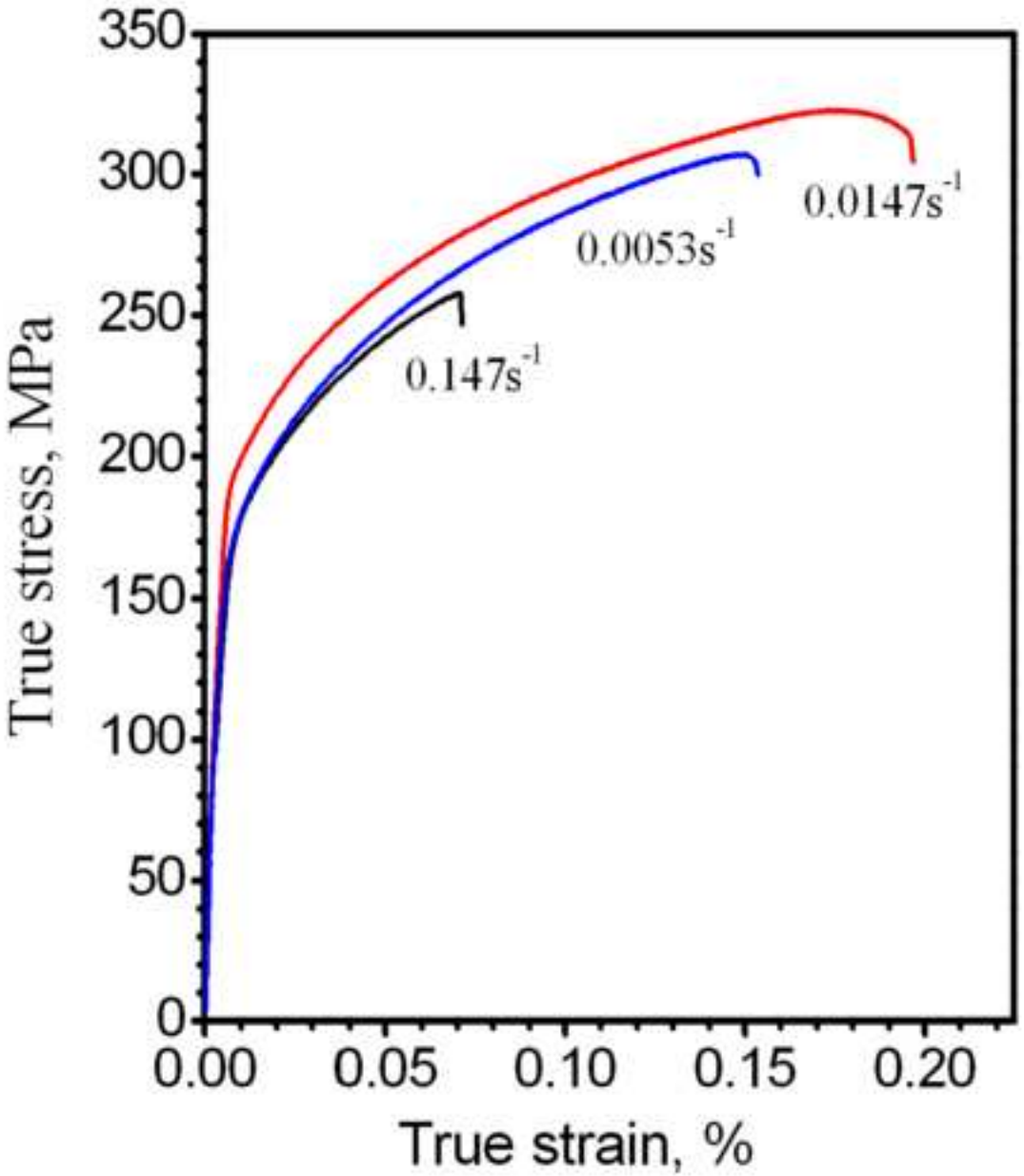

Figure(s)5a
Click here to download high resolution image

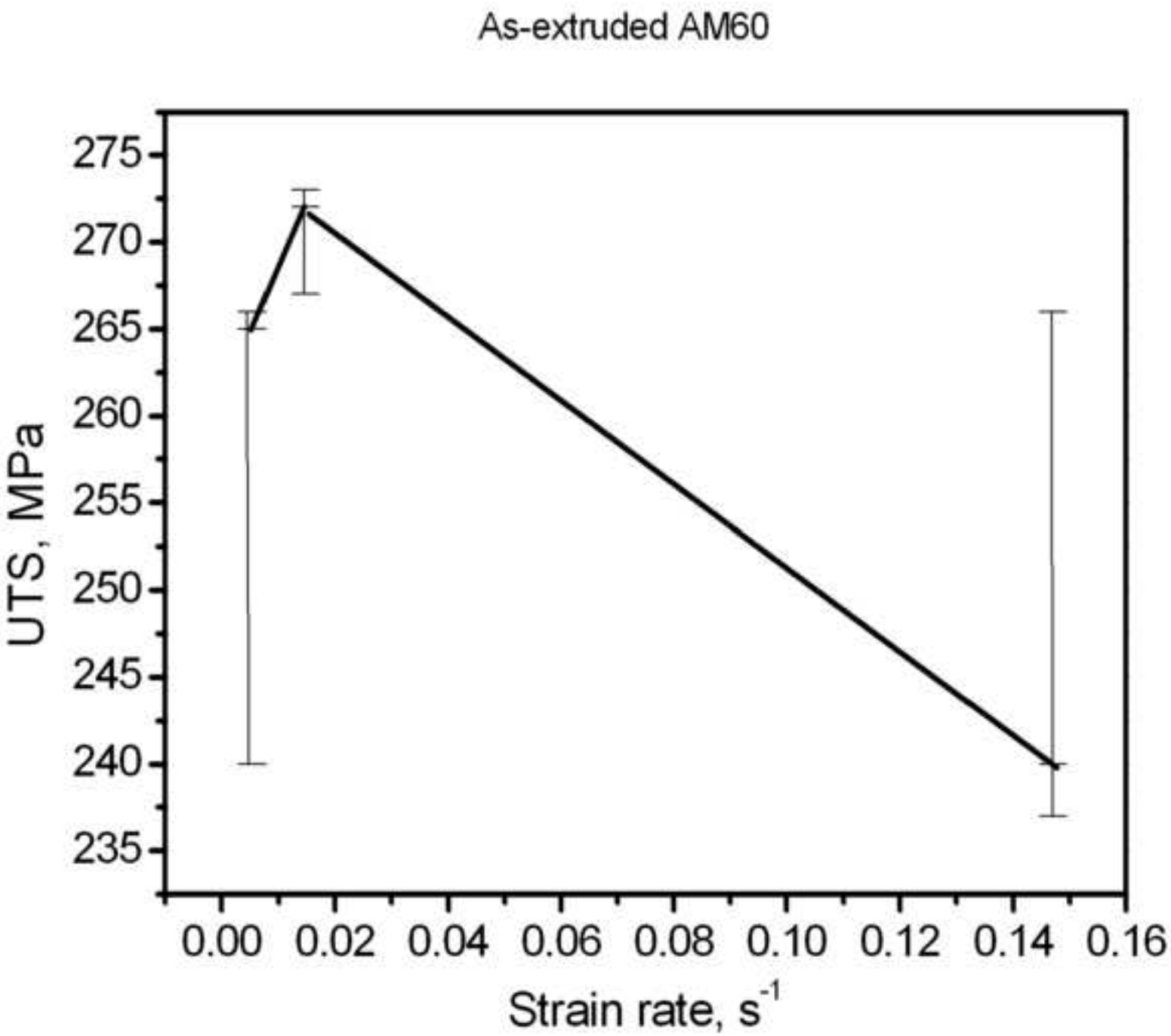

Figure(s)5b
Click here to download high resolution image

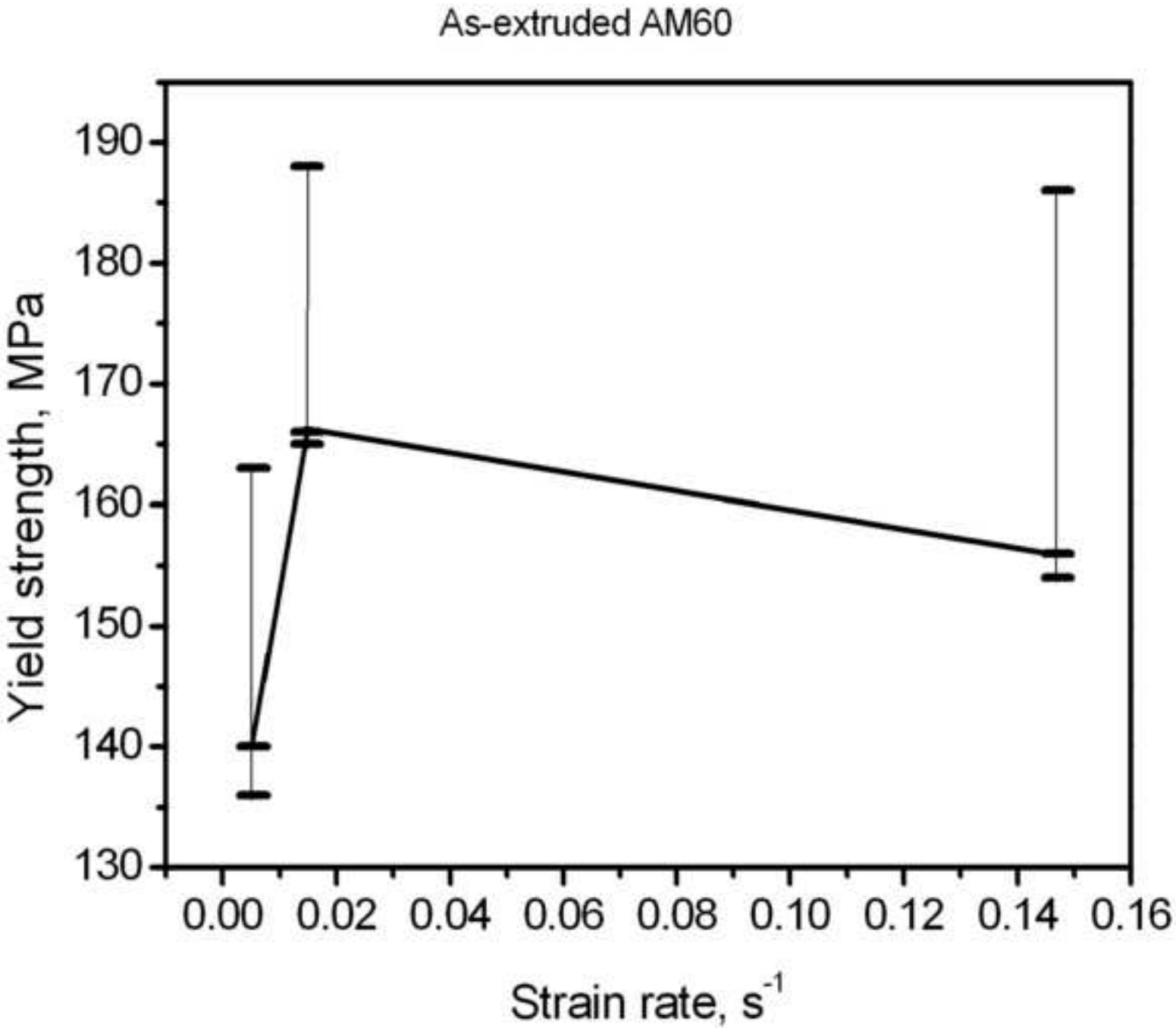

Figure(s)5c
Click here to download high resolution image

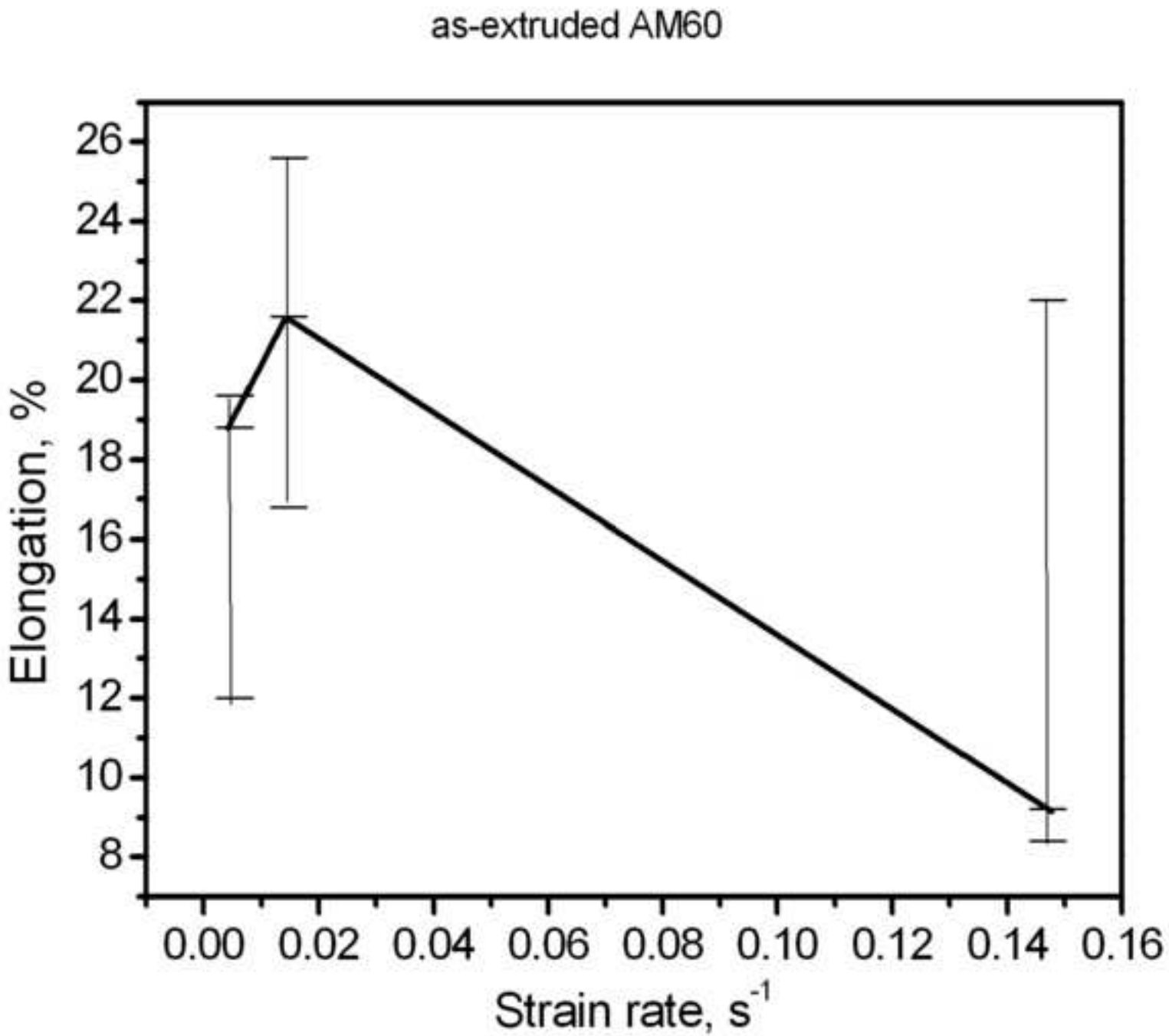

Figure(s)6

Click here to download high resolution image

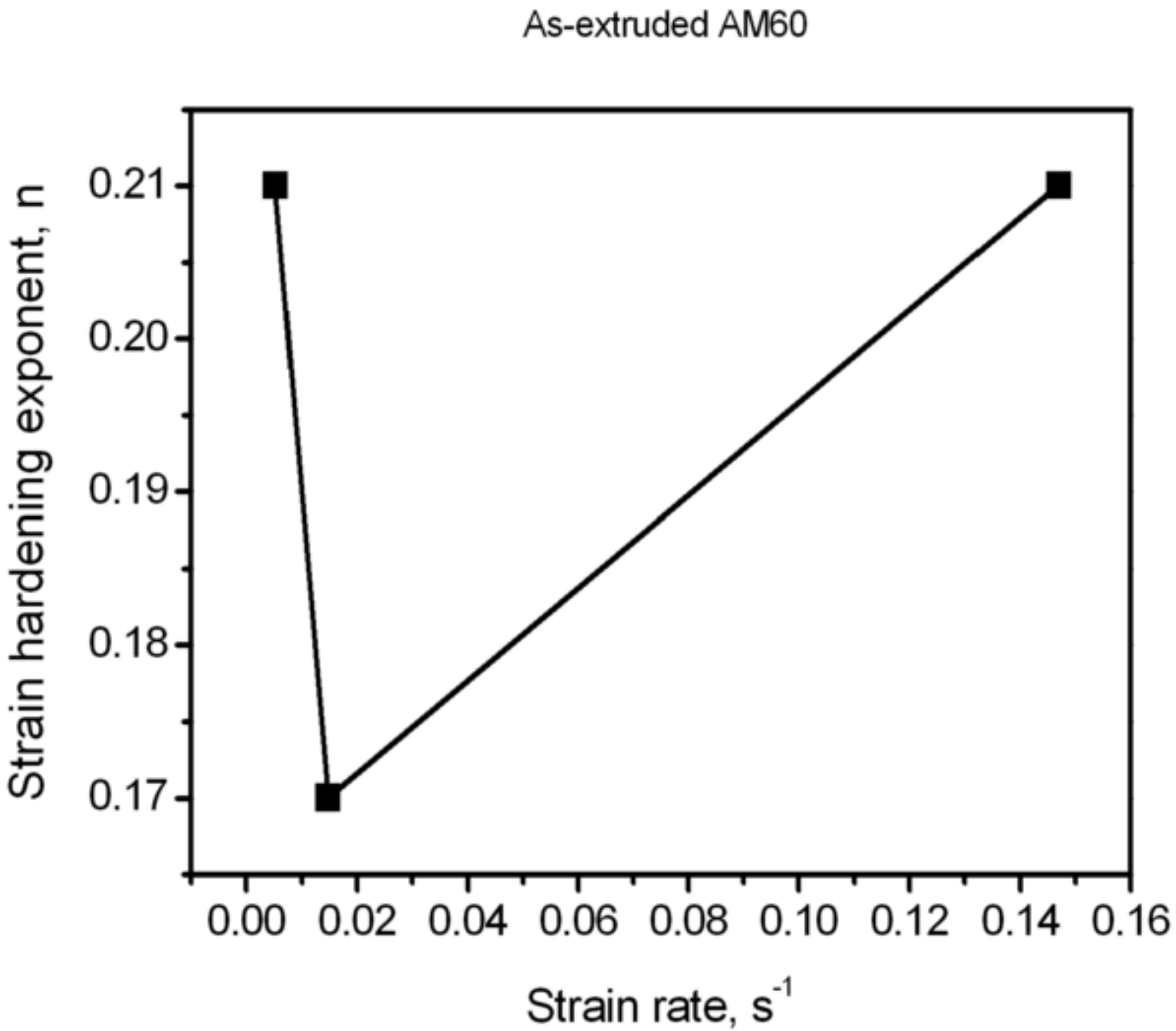

Figure(s)7
Click here to download high resolution image

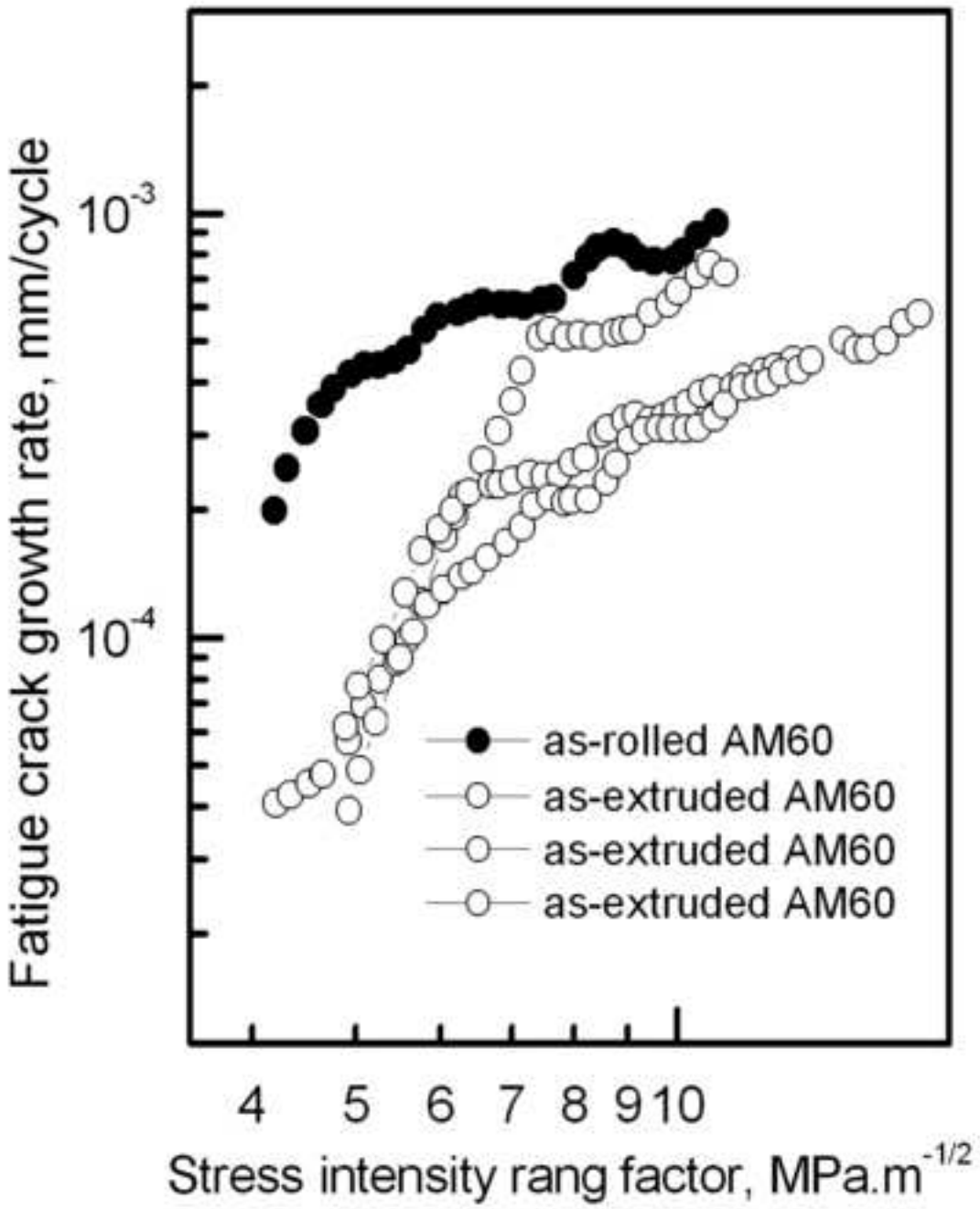

Figure(s)8a

Click here to download high resolution image

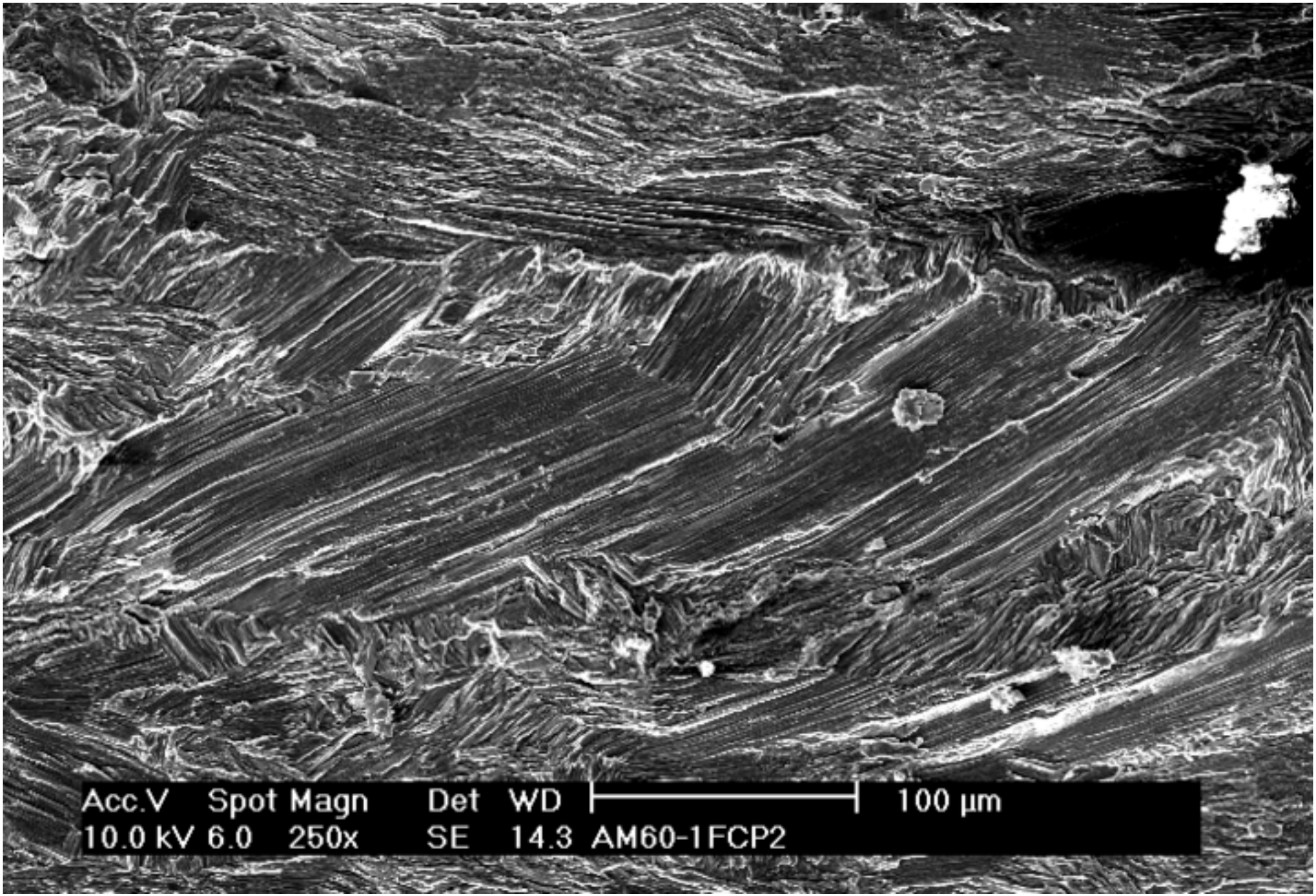

Figure(s)8b

Click here to download high resolution image

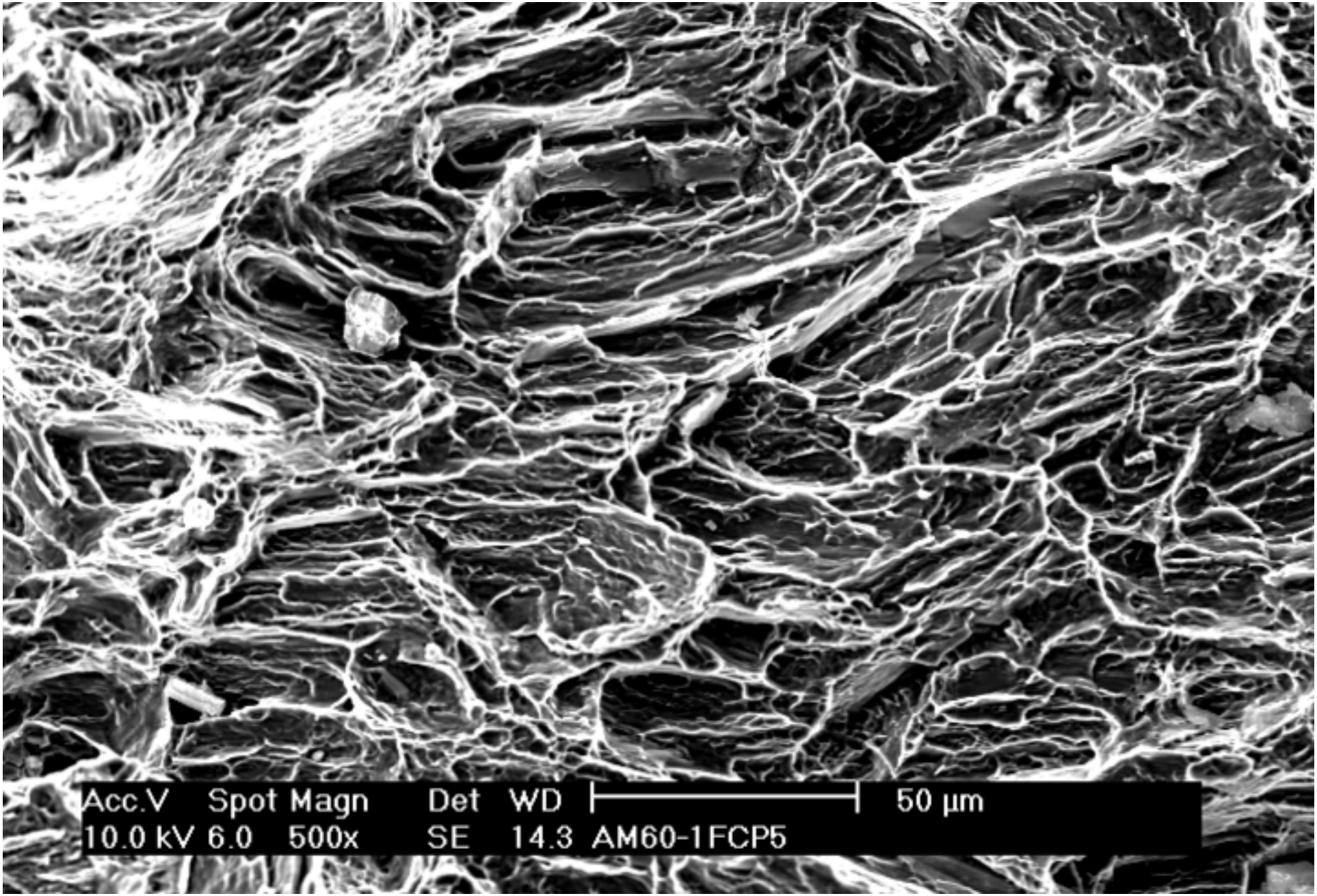

Figure(s)9a

Click here to download high resolution image

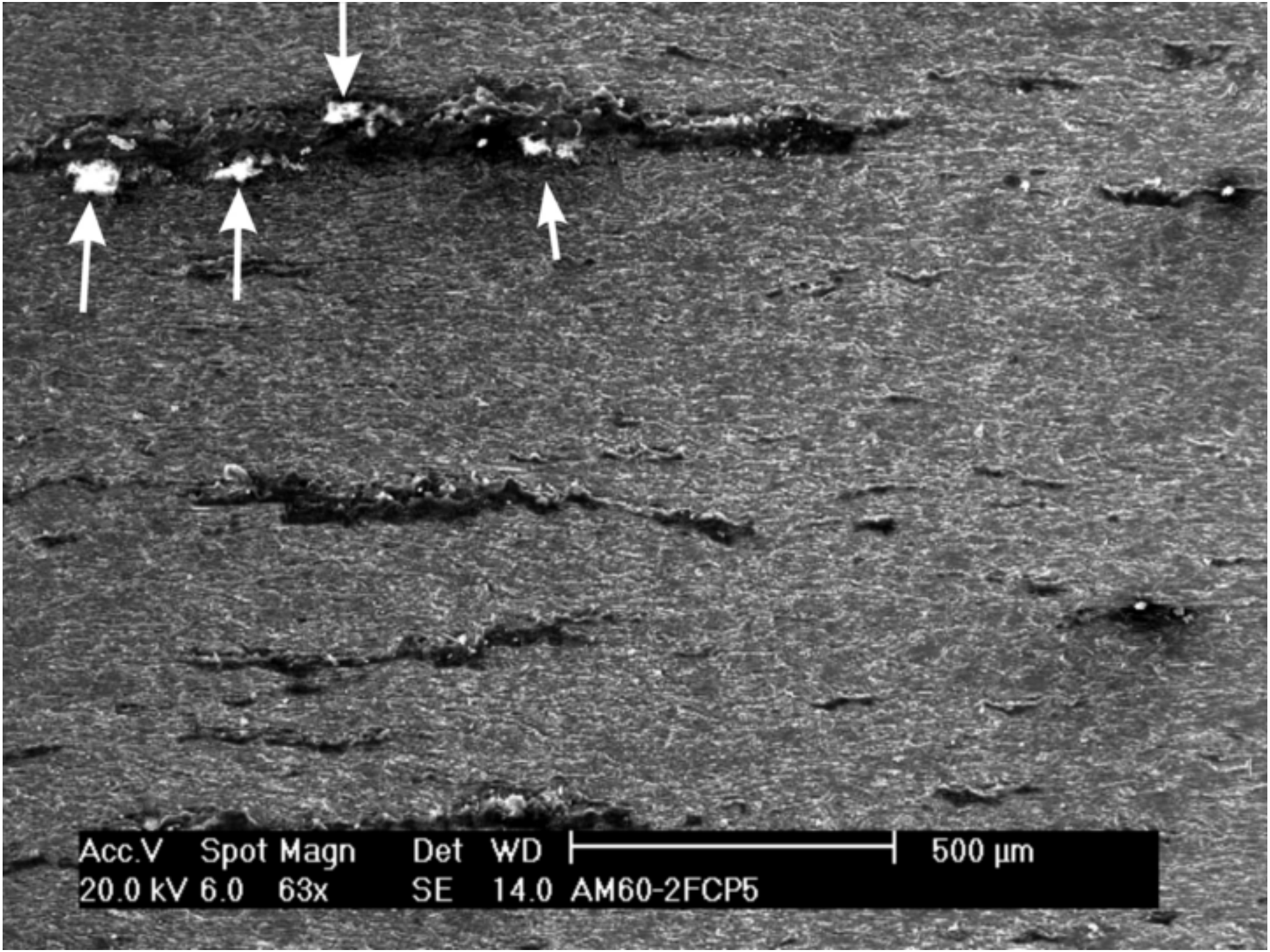

Figure(s)9b

Click here to download high resolution image

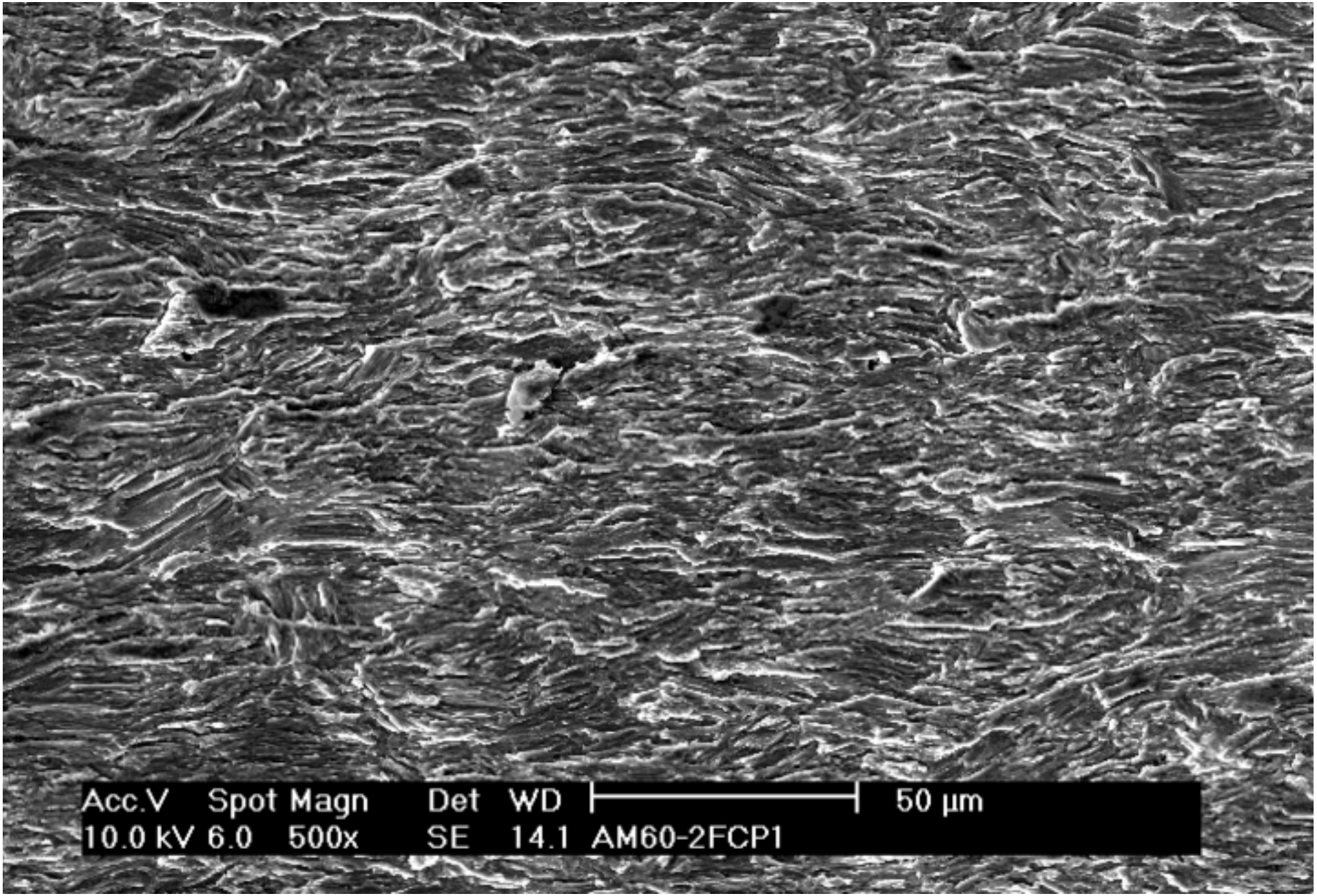

Figure(s)10

Click here to download high resolution image

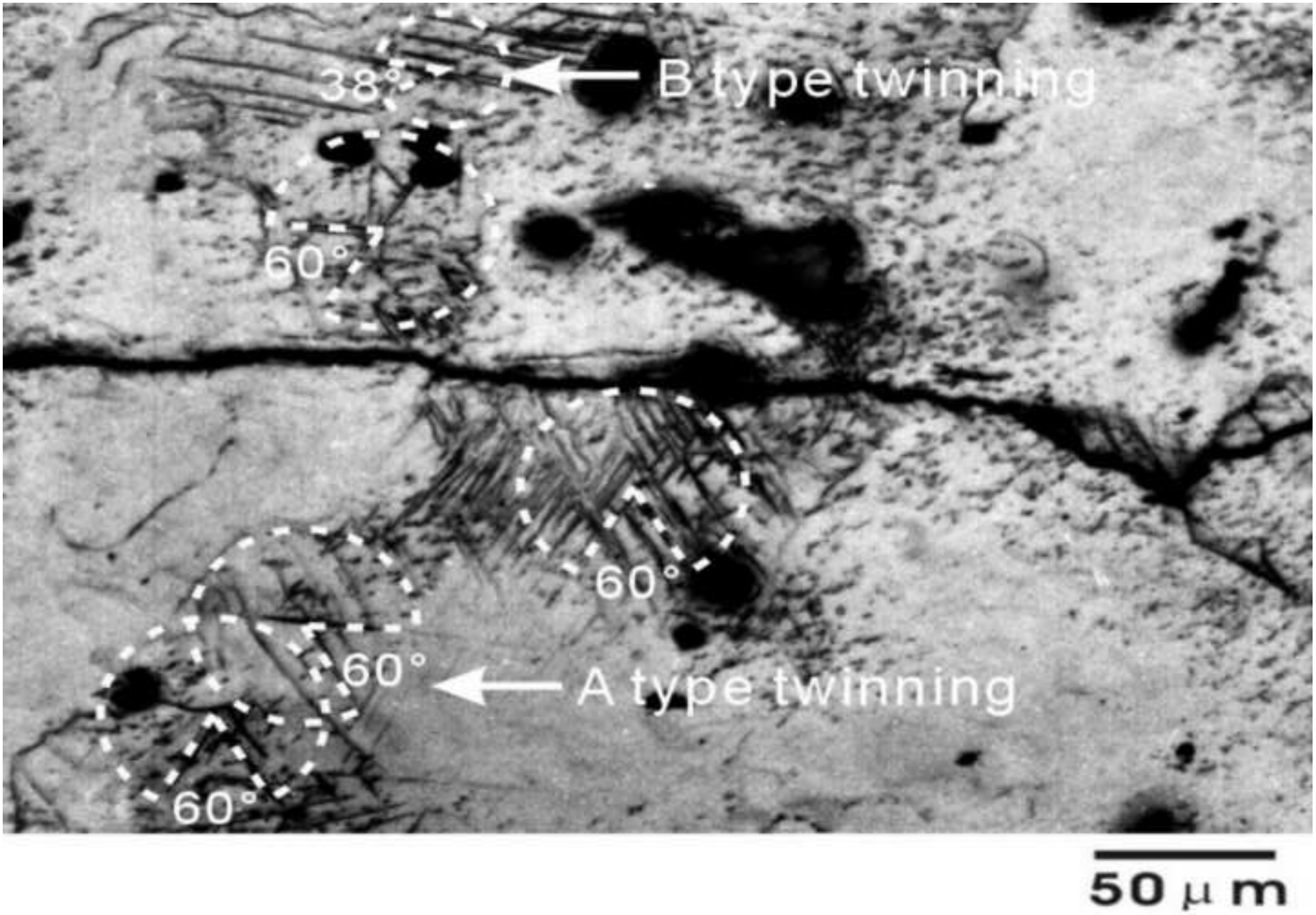

Figure(s)11a

Click here to download high resolution image

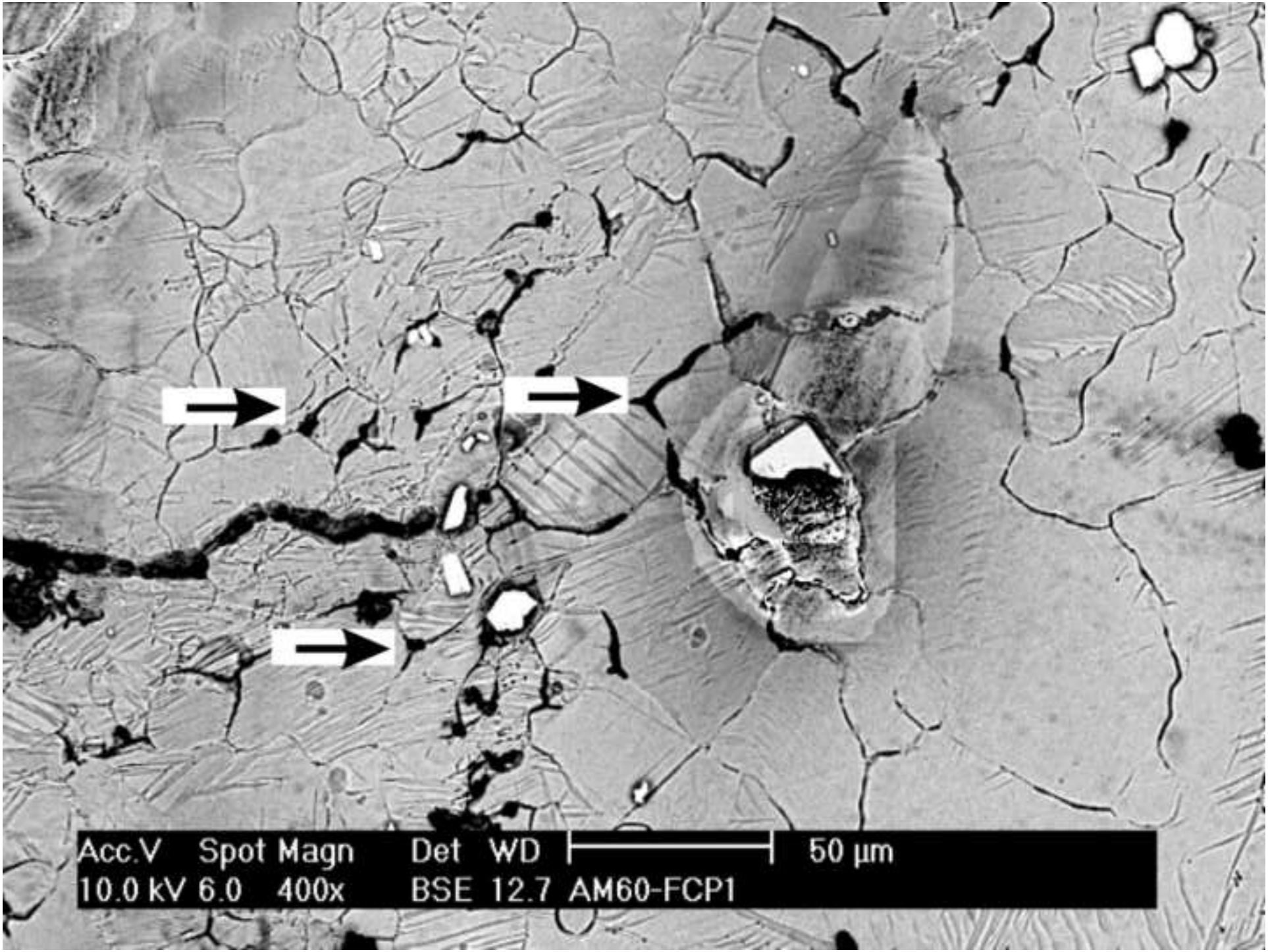

Figure(s)11b

Click here to download high resolution image

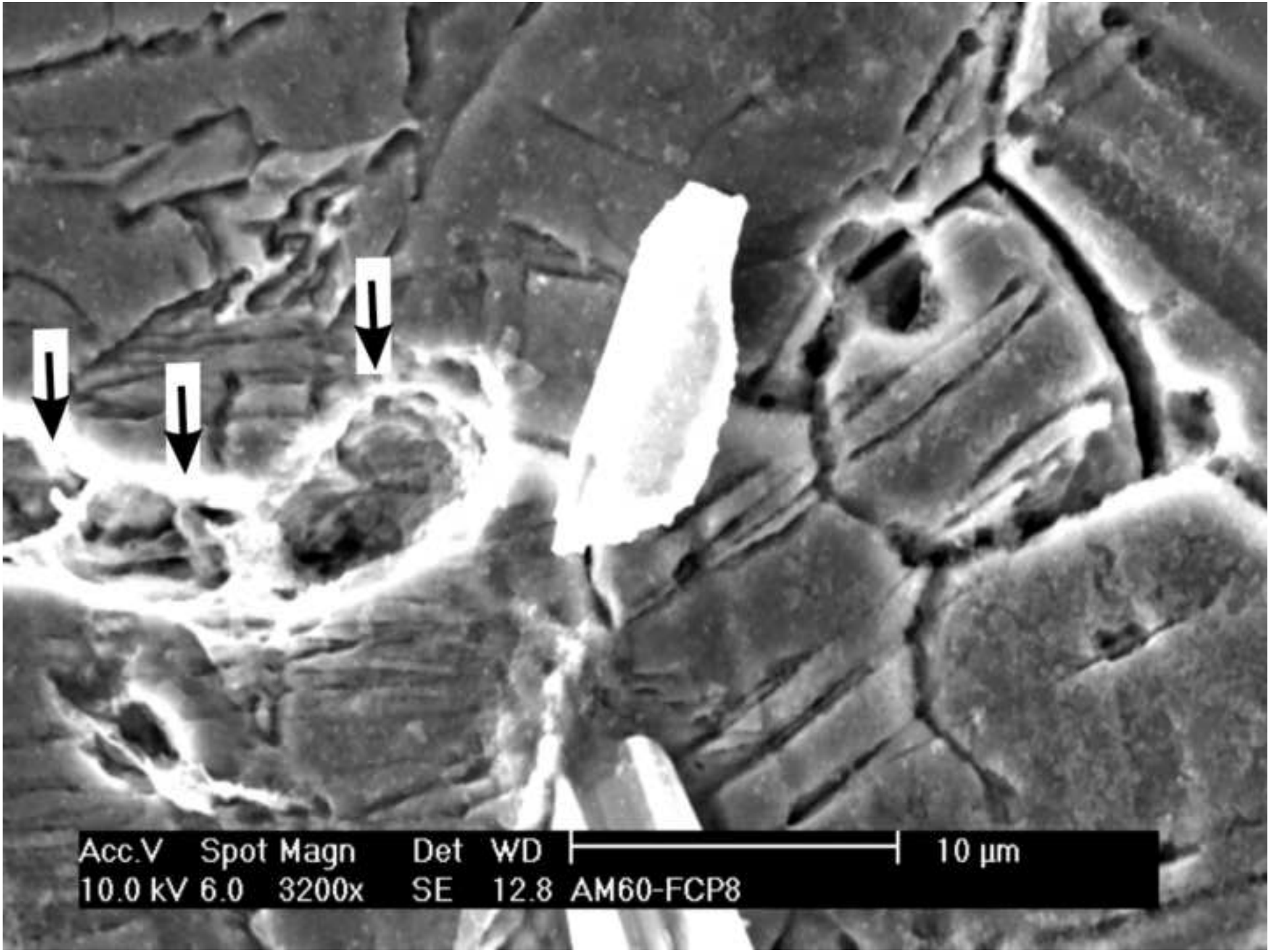

Figure(s)12a

Click here to download high resolution image

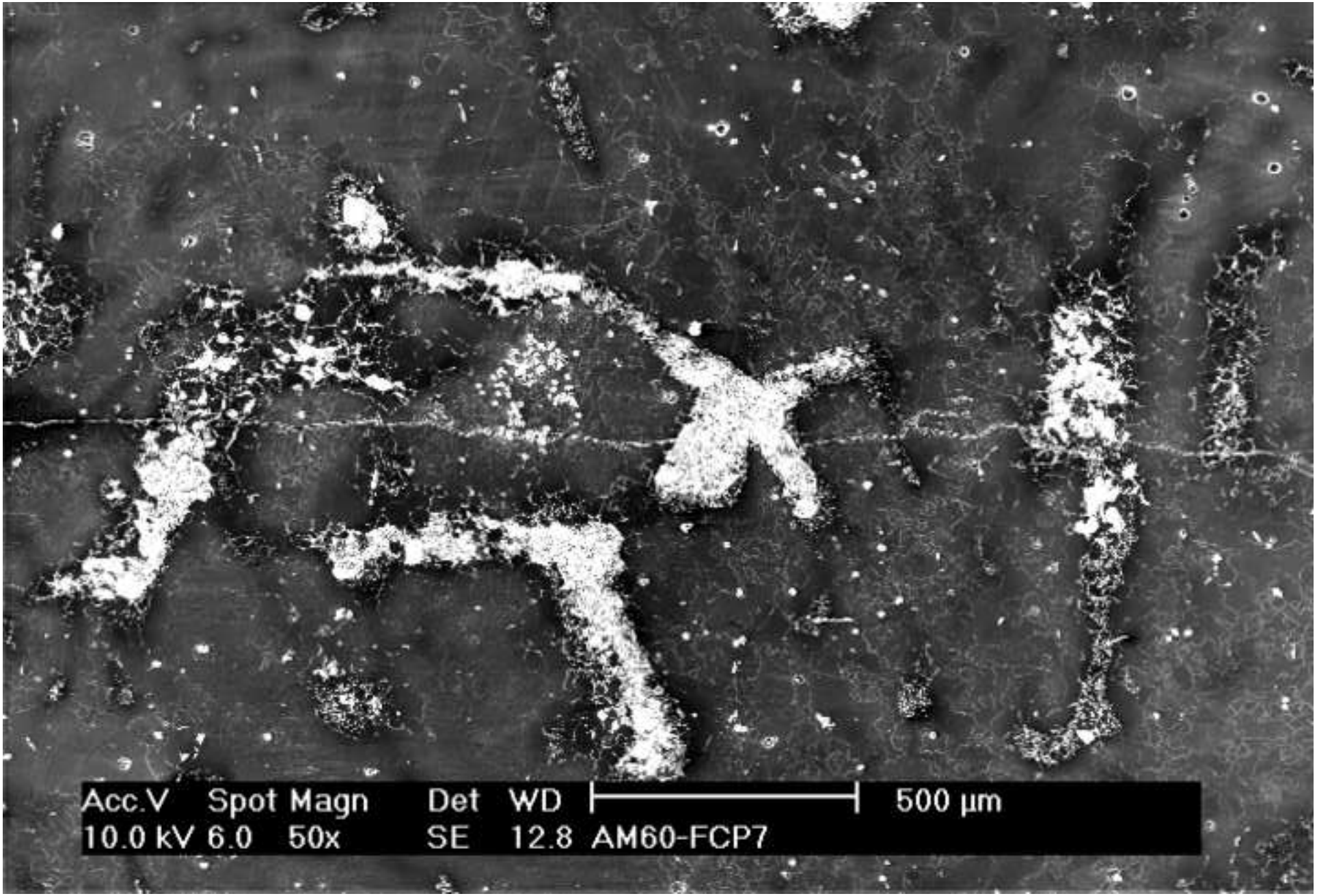

Figure(s)12b

Click here to download high resolution image

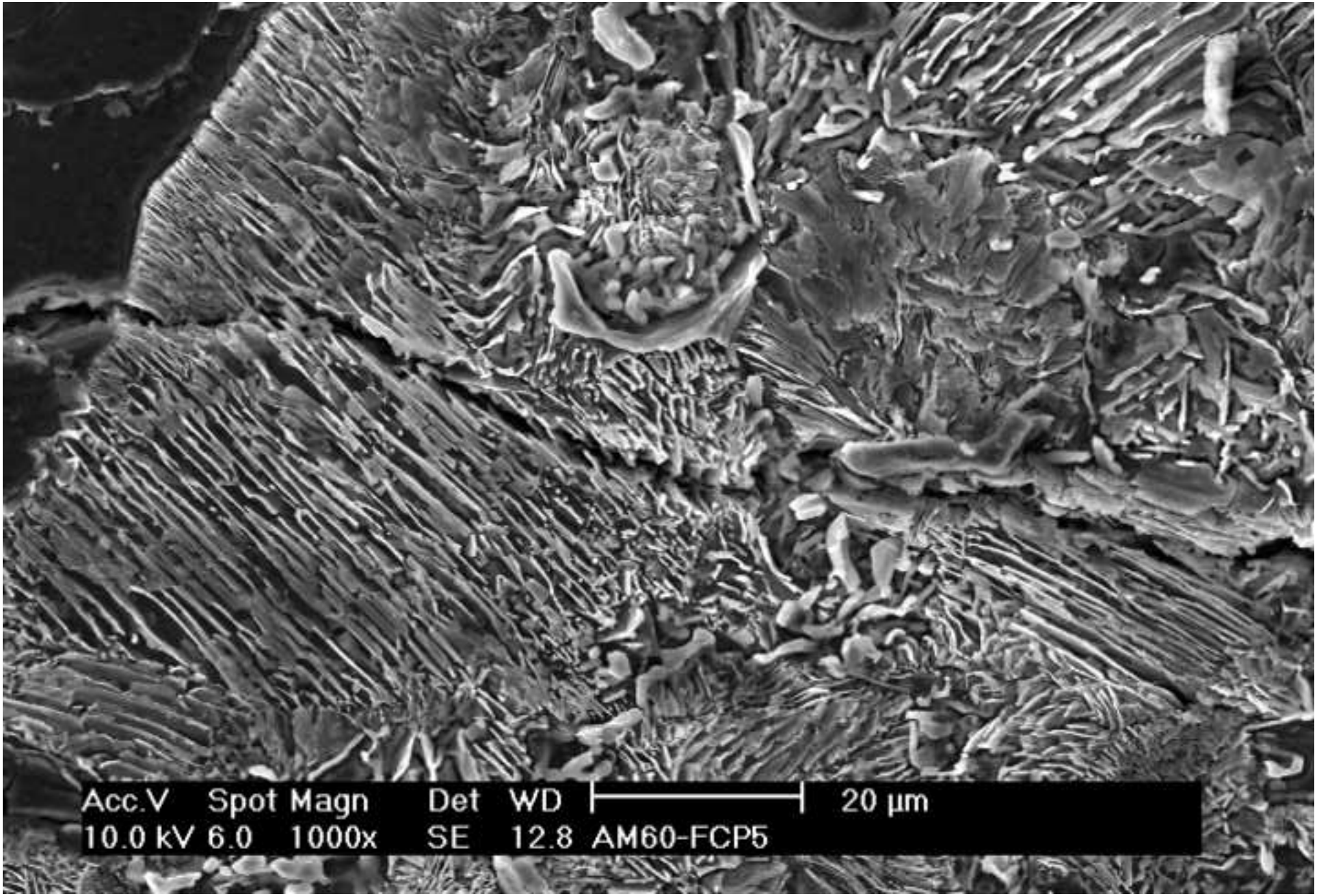

Figure(s)13a

Click here to download high resolution image

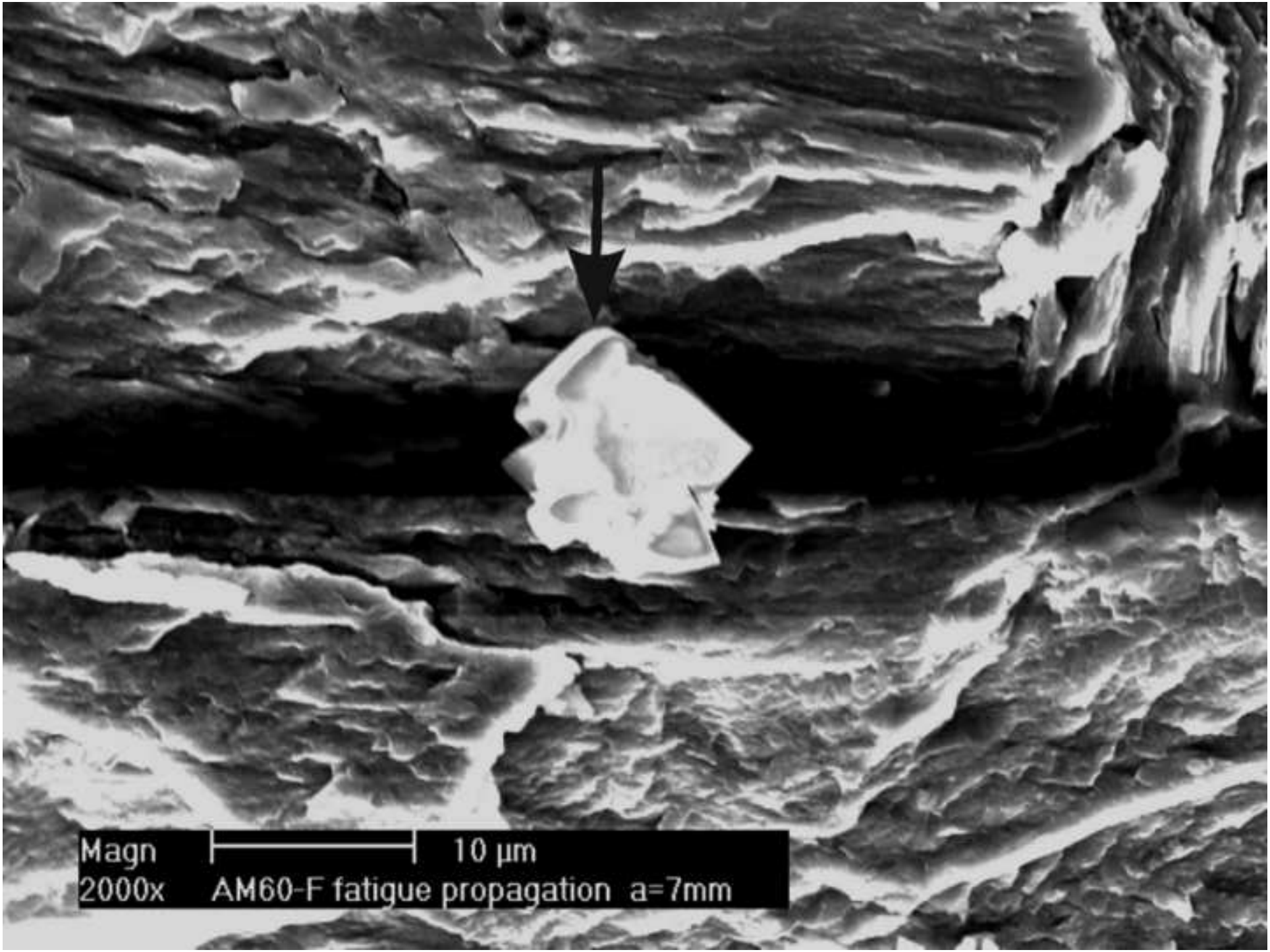

Figure(s)13b
Click here to download high resolution image

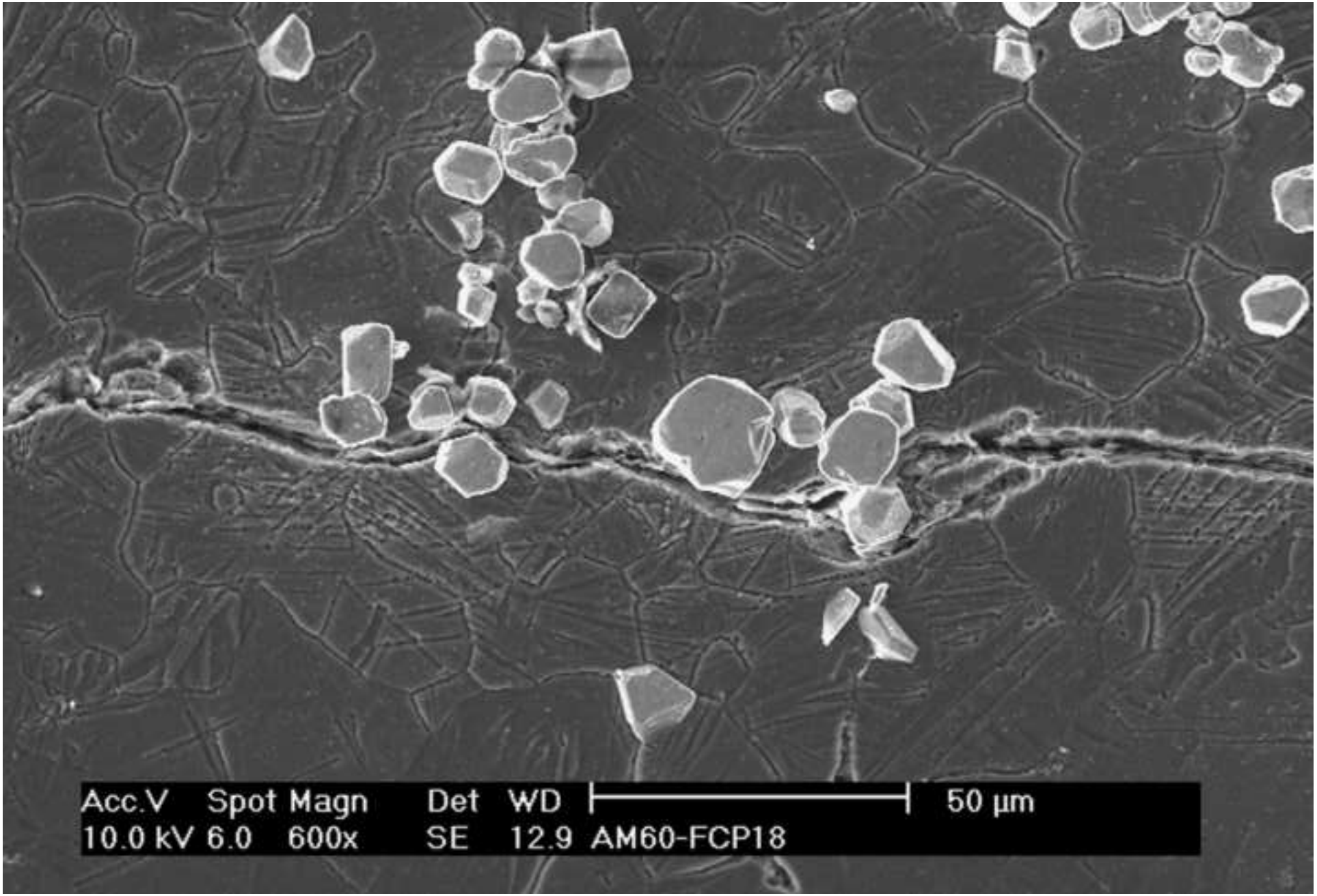

Figure(s)14

Click here to download high resolution image

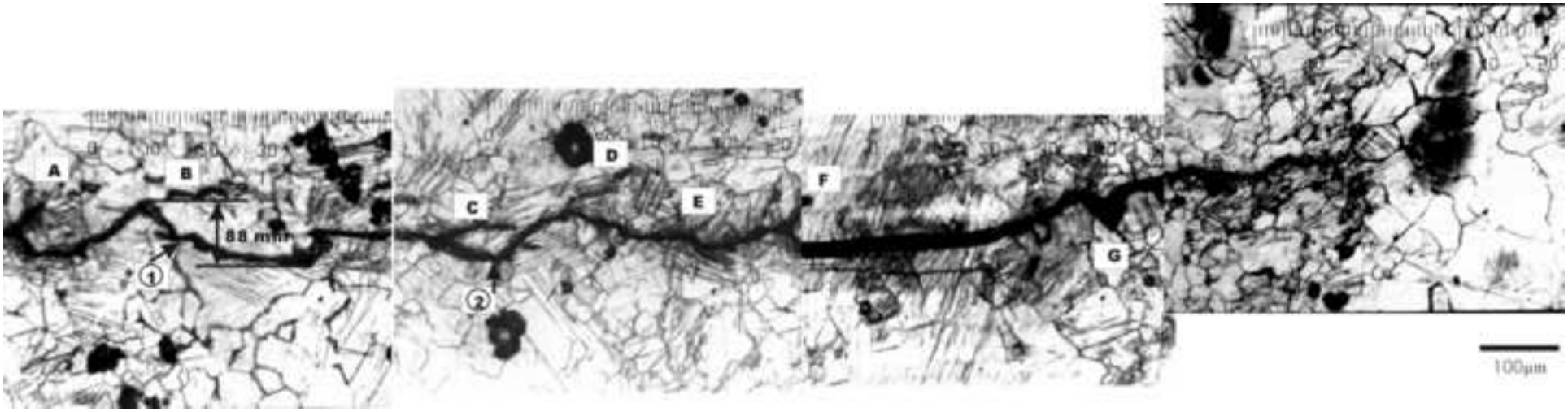

Figure(s)15

Click here to download high resolution image